SEMI-ANNUAL REPORT

October 1, 1967 - March 31, 1968

Emory University

NATIONAL AERONAUTICS AND SPACE ADMINISTRATION

Research Grant NGR-11-001-026

Principal Investigator: Norman A. Baily
Professor of Radiology

Distribution:

10 copies - Office of Grants and Research Contracts,
Attention: Code SC, NASA

1 copy - Dr. Leo Fox, NASA, OART, Biotechnology

1 copy - Dr. C. W. Malich, NASA, Ames Research Center

Introduction

The general aims of the research undertaken under this grant were:

1. To elucidate and clarify in a quantitative manner the transfer of energy from high energy protons to tissue in both macro and micro volumes.

2. To test the Blunck-Leisegang theory of the statistical distributions of small energy losses.

3. To develop methods by which physical data acquired using cyclotron generated protons may be used to predict the energy deposition patterns (macro and micro) in large animals or humans irradiated by specifically defined proton fields.

4. To collate radiobiological data which has been obtained using both whole animals and cells so that tolerance levels for manned space flight may be generated.

The work during the past six months was divided into two phases. The first concerned itself with the acquisition and construction of the equipment required to continue the cyclotron work initiated when the principal investigator was at the Hughes Research Laboratories.

A Nuclear Data 512 channel analyzer and all associated electronics (preamplifiers, amplifiers, power supplies, etc.) were acquired with non-grant funds. The proportional counters previously used were transferred from Hughes to Emory University. The equipment has been assembled and calibrated.

Large volume, small cross-section, p-i-n silicon detectors, to be used as coincidence detectors, were available from our previous work. The facility for making such units and others deemed to be necessary is available jointly between the departments of physics and radiology. This facility

makes possible the fabrication of lithium-drifted silicon structures in any desired geometry such as spheres, cylinders, and long path-length (1-5 cm) detectors formed in parallelepiped geometries.

The photomultiplier, preamplifier, and light pipe system for use with plastic scintillating spheres were also transferred from Hughes to Emory. No work using this system was performed during this reporting period.

Tissue-equivalent absorbers were constructed for use with the tissue-equivalent proportional counter, so that micro-dose distributions at various tissue depths can be studied.

A student has been employed to collate all available proton radiobiological data from the open literature, conference reports, and both the internal and contract reports of government laboratories and contractors. These will be compiled as a function of biological sample and proton energy. Data for absorbed dose less than 25 rad and greater than 10^3 rad will be deleted. This material will then be analyzed for dose-rate effects and the influence of the geometrical distribution on both the macro and micro dose patterns existing within the irradiated material.

Isodose Patterns

Utilizing experimental data,[1] the distribution of absorbed dose within

---

1. R. L. Tanner, N. A. Baily, and J. W. Hilbert, "High-Energy Proton Depth-Dose Patterns," Rad. Res. 32, 861-874 (1967).

---

cylindrical tissue-equivalent phantoms delivered by various energy proton beams has been examined for certain geometrical fields, corresponding to broad-beam cyclotron irradiations in which the phantom is rotated about a central point. Pure proton beams ranging in energy from 45.8 MeV to 730 MeV

were considered. These were assumed to be incident perpendicularly to the cylinder axis and uniform about it. Similar calculations were also undertaken for a 730 MeV beam degraded by 229 g/cm^2 copper and 199 g/cm^2 carbon whose depth-dose characteristics are quite different than those of pure proton beams. These differences in depth-dose characteristics are most certainly due to the production of secondary neutrons and γ-rays by the primary protons in their passage through the degraders. The text of a paper on this subject which has been prepared for publication is presented in Appendix A.

The computer program utilized was written in Fortran IV (G-level). The input consisted of the depth-dose data and the equation of the elliptical cylinder with variable major and minor axes.

Five to twenty-five points were chosen such that the differences between successive points on the depth-dose curves could be considered linear. These values were then read into a core array.

For each set of data, the depth-dose array was searched for two (2) values of the depth bracketing the value desired. The dose was then ascertained through linear interpolation.

To compute the total dose at any point within the cylinder, radii were erected from this point at intervals of 5°. The length of each radius (extending from the point under consideration to the surface) was then calculated. This distance (along each radius) was then used to determine the central axis depth dose to that point delivered by an infinitely large field whose axis was parallel to the radius. The seventy-two individual values were then summed and the sum multiplied by the angle increment ($\pi/36$) to obtain the total dose delivered to the point.

To determine the isodose lines, the total dose was calculated at equal increments of distance along the major axis. The program used the center of the ellipse as a starting point. For example, starting along the major axis, when the dose at two consecutive points is found to bracket the desired value of the isodose contour being sought, a linear interpolation is performed to find the intersection of this isodose curve with the major axis. A vector is then erected at this point perpendicular to the axis and the dose computed at its end. The vector is then rotated and the dose at the new point now marking its end computed. Should this value be farther from the desired value, the sense (or direction) of vector rotation is reversed. When the values of the dose at the ends of two such vectors bracket the desired value of the isodose line being sought, a linear interpolation of the angle is performed. This point is then taken as a new starting point, a new vector erected, and the last angle and sense of rotation utilized in a new search. The process is automatically terminated when either axis of the cylinder or its surface is encountered, or if no pair of vectors can be found bracketing the value of the desired isodose line.

All pertinent parameters were displayed on the CRT of an IBM-2250 mod 2 display console and could be changed by the operator through the use of the light pencil. Vector lengths used usually ranged from 0.2 to 1.0 cm. The increments of angle were adjusted in the range of 0.1 to 0.3 radians. Both depth-dose and isodose curves were displayed. Values on a 1 cm x 1 cm grid were printed out in the usual manner.

The computer used was a 102K partition of the IBM - 360/75 at the UCLA Health Sciences Computing facility. Graphics management was accomplished using 8K of buffer and GRAF language.

Cyclotron Experiments

Six days of parasite running time was assigned to the Emory group by the director of the SREL, during the period of March 19 through 24. A low-intensity, 600 MeV proton beam was selected by a bending magnet and delivered to the experimental area.

Experiments designed to extend the experimental data on energy event frequency distributions to very small values of K (< 0.001) and to large values of b^2 (> 25) were designed.

Data was acquired for pathlengths of 1.33×10^{-3} g/cm^2, 6.66×10^{-4} g/cm^2, 3.33×10^{-4} g/cm^2, 1.33×10^{-4} g/cm^2, 9.95×10^{-5} g/cm^2, 6.66×10^{-5} g/cm^2, and 3.33×10^{-5} g/cm^2.

At this date, no analysis of the experimental data has been accomplished.

Microdosimetric Distributions

Energy deposition distributions for one simulated pathlength, equivalent to 1.18 microns of tissue, were measured at various depths in Shonka tissue-equivalent plastic, for portons with an incident energy of 43.0 MeV. These distributions were obtained by recording the pulse height distributions due to passage of the protons across a diameter of a spherical tissue-equivalent proportional counter, described in previous reports, operating at a gas pressure of 20 Torr, and placing various thicknesses of tissue-equivalent plastic flush with the outer shell of the counter. Actually, two different types of distributions may be obtained in this manner. For illustrative studies such as the present one, it is of particular interest to determine such distributions for an essentially monoenergetic incident proton beam. Such distributions are obtained using a coincidence technique. In many practical situations,

however, biological exposures cannot be performed in a strictly mono-energetic beam. In fact, the procedures used to spread cyclotron proton beams may result in a proton spectrum with a not insignificant low energy tail below the main energy peak. A fairly typical proton energy spectrum, measured with a p-i-n semiconductor detector, is shown in Figure 1 (the spectrum is actually that after passage of 44 MeV protons through the two walls of the tissue-equivalent plastic counter). This spectrum shows about 45% of the total proton flux in the low energy tail. However, just how much of the tail in this particular case is actually due to lower energy protons produced by the beam spreading procedure is not known. A considerable fraction is very probably due to passage of peak energy protons obliquely through the semiconductor detector, since only a rather crude collimator was used in front of the p-i-n. At any rate, whenever a significant low energy tail is unavoidable in a biological exposure situation, the corresponding microscopic absorbed energy distribution of interest is obviously that due to the entire proton spectrum with which the biological sample is irradiated. In such a case, the distribution of energy deposition for a given pathlength may be obtained by simply placing a well designed collimator in front of the proportional counter to produce a pencil-like beam of protons. Distributions of this type were also measured as a function of depth in tissue-equivalent plastic, using a collimator with an area of $\simeq 0.2$ cm^2.

1.18 microns of tissue is simulated by the gas path along a diameter of the proportional counter when it is operated at a pressure of 20 Torr. This simulates 1.18 microns of tissue in the sense that the same average energy is lost in traversing the gas path and, because of the approximate equality in electron densities, quite similar energy-loss distributions

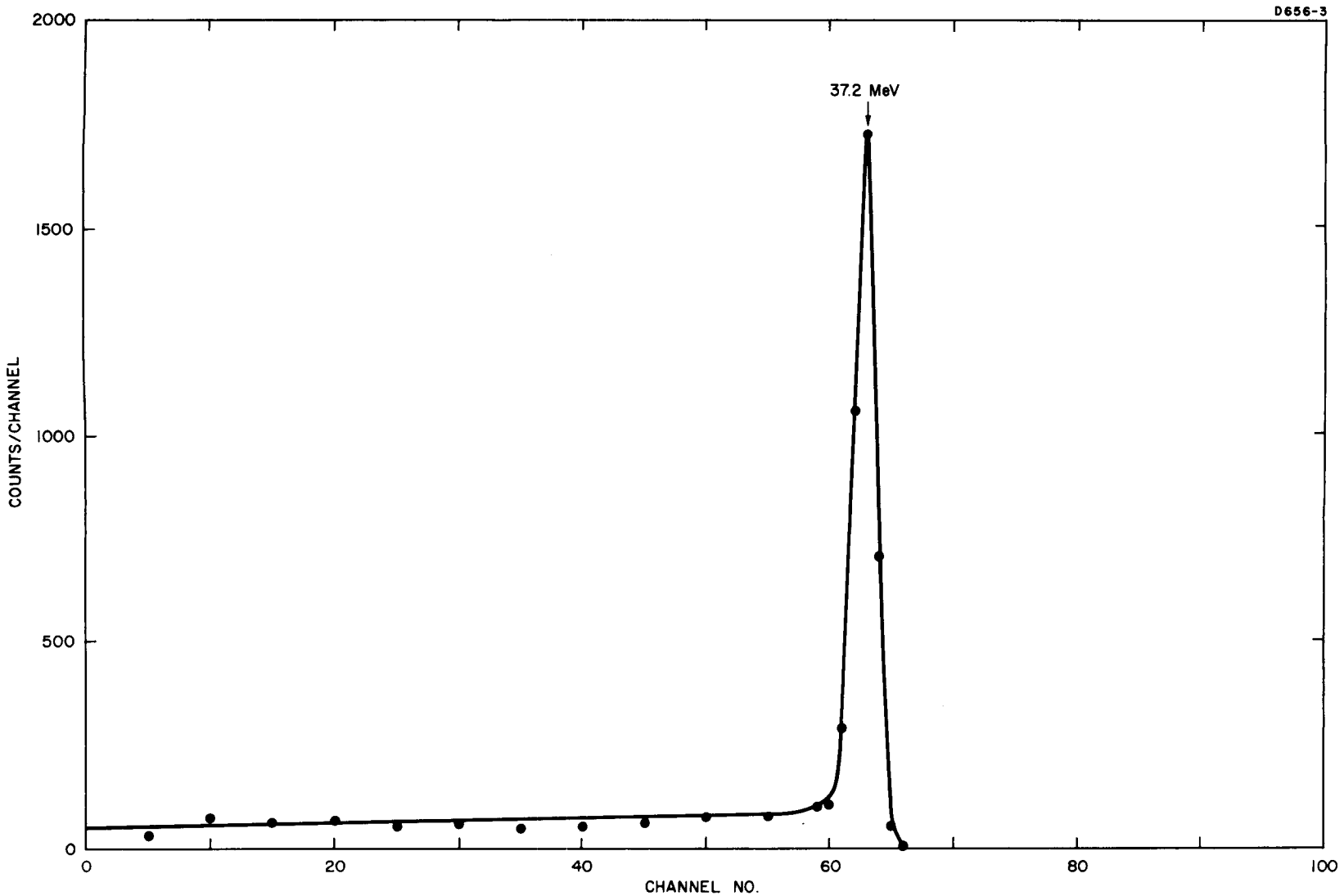

Figure 1. Typical energy spectrum of a spread proton beam (44 MeV maximum incident energy after passage through $\simeq$ 0.40 g/cm^2 of tissue-equivalent plastic).

are predicted (i.e. if the electron densities were markedly different, the predicted energy-loss distributions, for the same average energy loss, would be quite different). Since the ratio of the mass stopping power of tissue to the mass stopping power of the He-CO_2 gas mixture changes very little in the energy range of interest (< 3% change from 50 to 2 MeV), the "equivalence factor" relating g/cm^2 of He-CO_2 to g/cm^2 of tissue may be taken to be a constant.[2] Since the relative mass stopping power of

---

2. W. H. Barkas and M. J. Berger, "Tables of Energy Losses and Ranges of Heavy Charged Particles," Studies in Penetration of Charged Particles in Matter, NAS-NRC Publ. no. 1133, 103 (1964).

---

tissue to the He-CO_2 mixture is approximately 1.13 in this range, 1.33×10^{-4} g/cm^2 of He-CO_2 (density of the mixture at 20 Torr pressure x pathlength in the counter) simulates $1.33 \times 10^{-4}/1.13 = 1.18 \times 10^{-4}$ g/cm^2, or 1.18 microns, of tissue.

Figures 2-6 show both coincidence spectra for protons with an incident energy of 43.0 MeV, and, for illustrative purposes, non-coincidence (collimated) spectra for a proton spectrum with a peak at 43.0 MeV. Figures 2, 3, and 4 compare the two types of distributions for depths of 0.20, 0.60, and 1.44 g/cm^2 of tissue-equivalent plastic, respectively. Figures 5 and 6 show only collimated proton beam distributions, since at these depths (1.58 g/cm^2 and 1.66 g/cm^2, respectively) the residual proton energies were insufficient to penetrate the back tissue-equivalent wall of the proportional counter and reach the p-i-n detector. At a depth of 1.71 g/cm^2, essentially no protons penetrated to the sensitive gas volume. This observation is in good agreement with the calculated

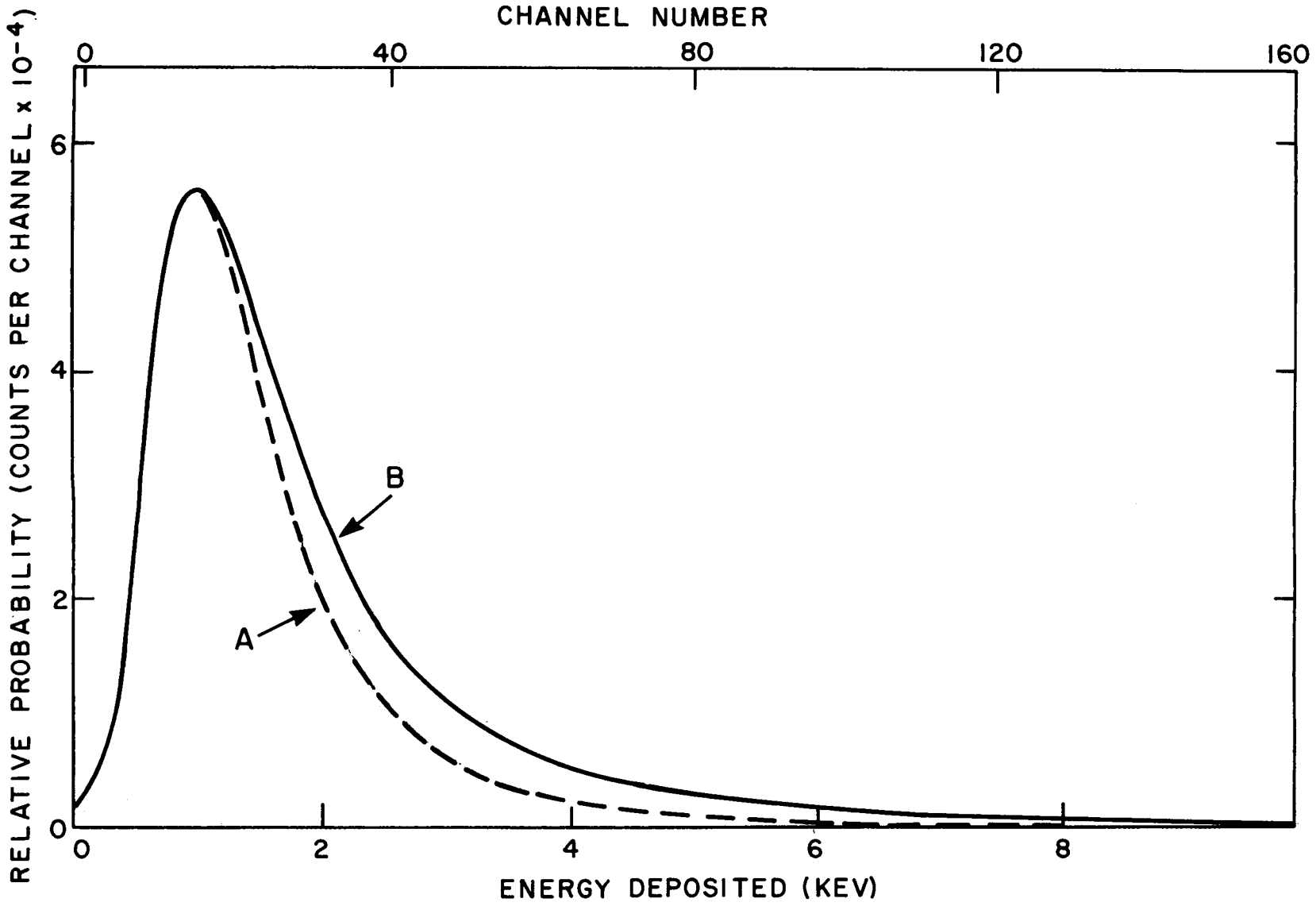

Figure 2. Energy deposition distributions in simulated 1.18 micron tissue-path, due to protons which have penetrated to a depth of 0.20 g/cm^2 in tissue-equivalent plastic. A = coincidence spectrum, due to 43.0 MeV incident protons. B = collimated beam spectrum, due to an incident proton energy spectrum with a peak at 43.0 MeV.

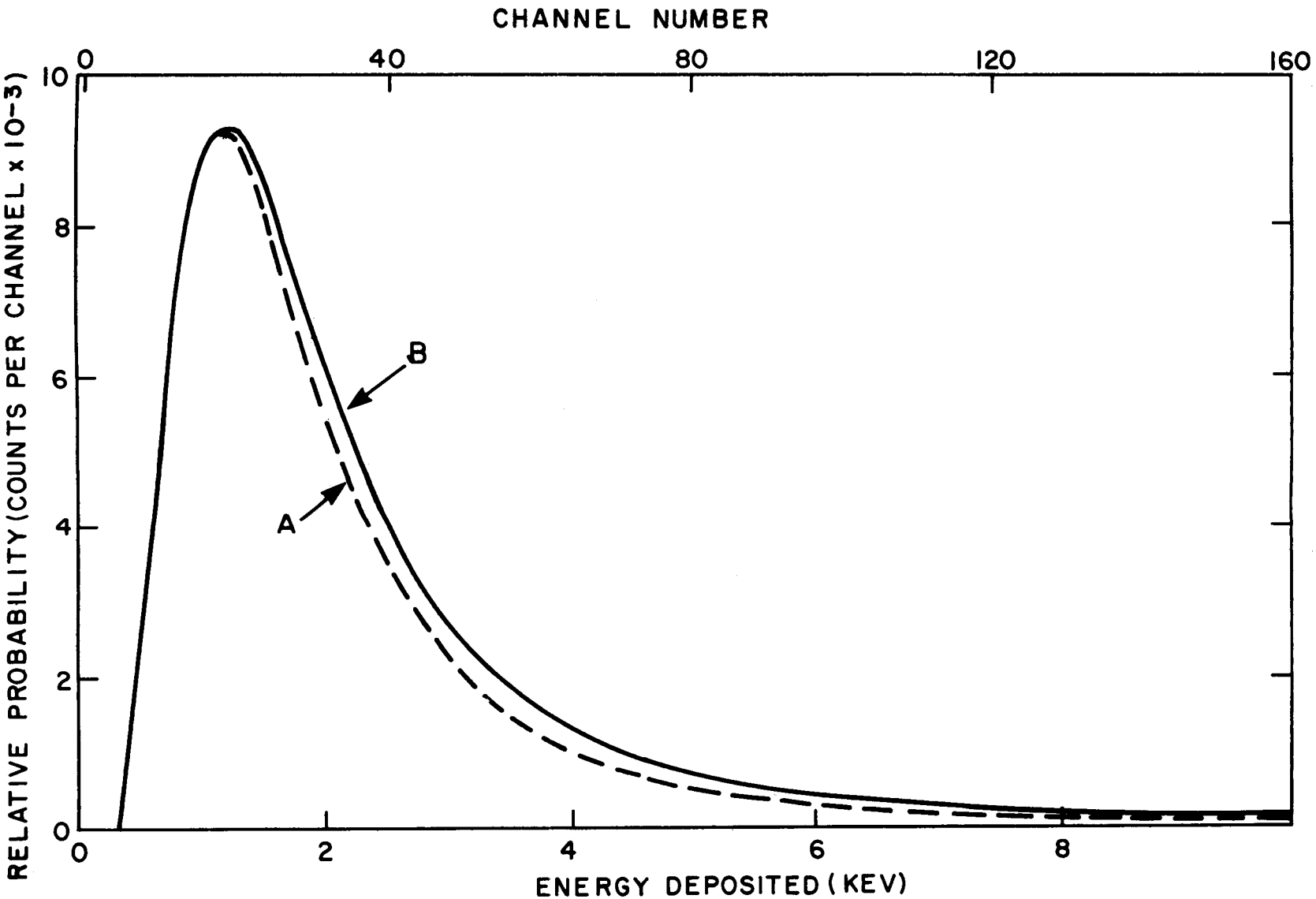

Figure 3. Energy deposition distributions in simulated 1.18 micron tissue-path, due to protons which have penetrated to a depth of 0.60 g/cm^2 in tissue-equivalent plastic. Curves A and B are as in Figure 2.

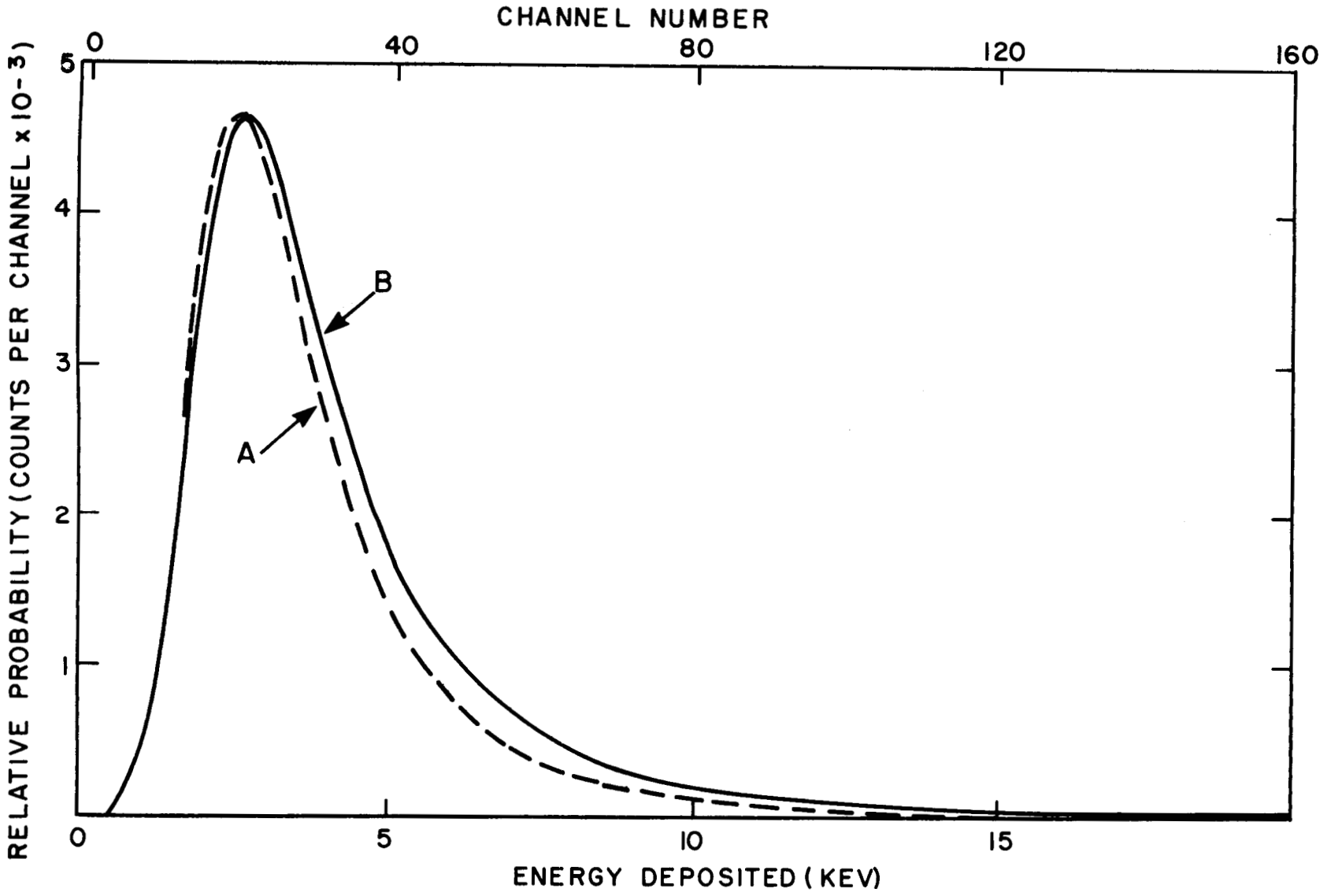

Figure 4. Energy deposition distributions in simulated 1.18 micron tissue-path, due to protons which have penetrated to a depth of 1.44 g/cm^2 in tissue-equivalent plastic. Curves A and B. are as in Figure 2.

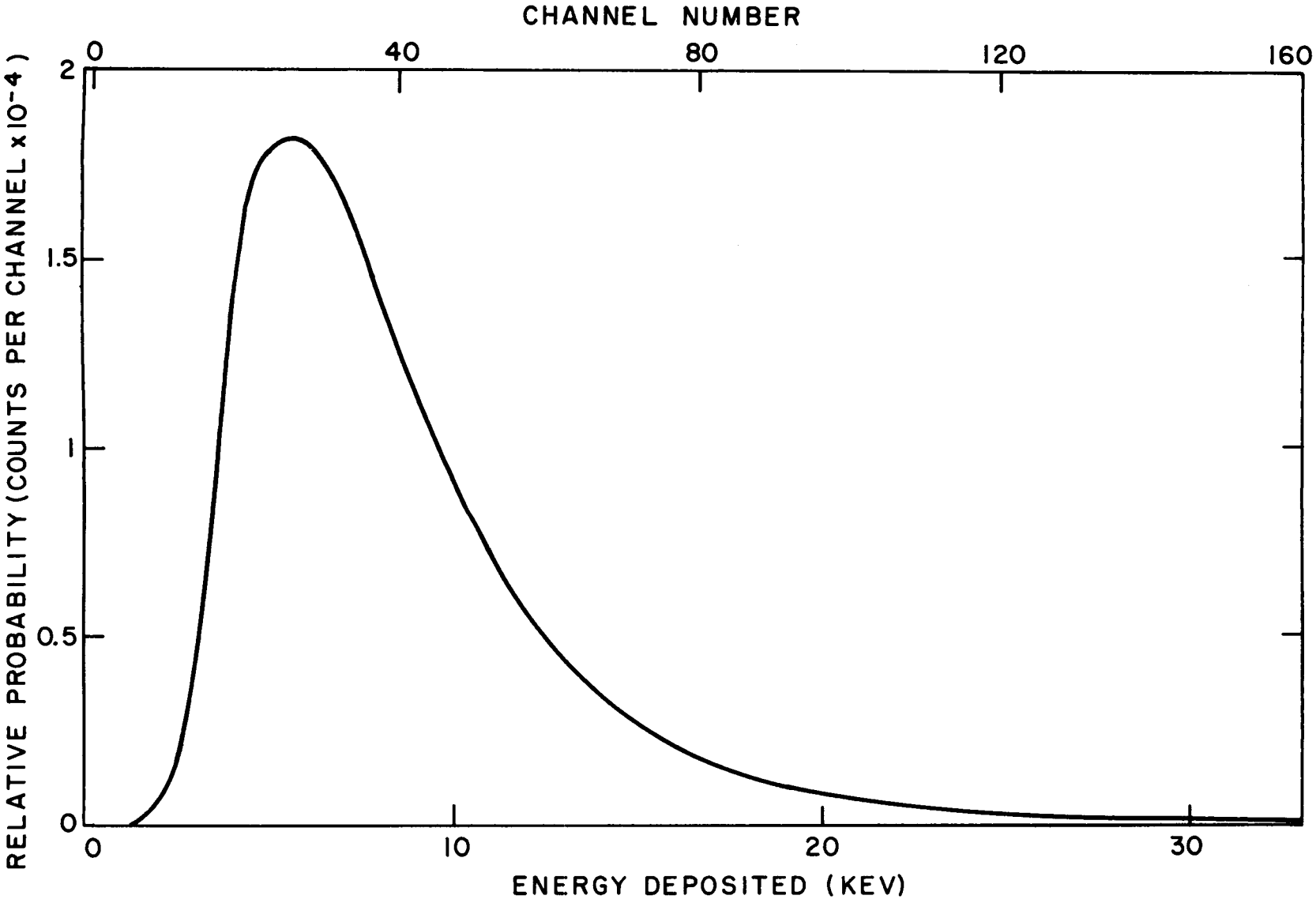

Figure 5. Energy deposition distribution in simulated 1.18 micron tissue-path, due to an incident proton energy spectrum with a peak at 43.0 MeV which has penetrated to a depth of 1.58 g/cm^2 in tissue-equivalent plastic (collimated proton beam).

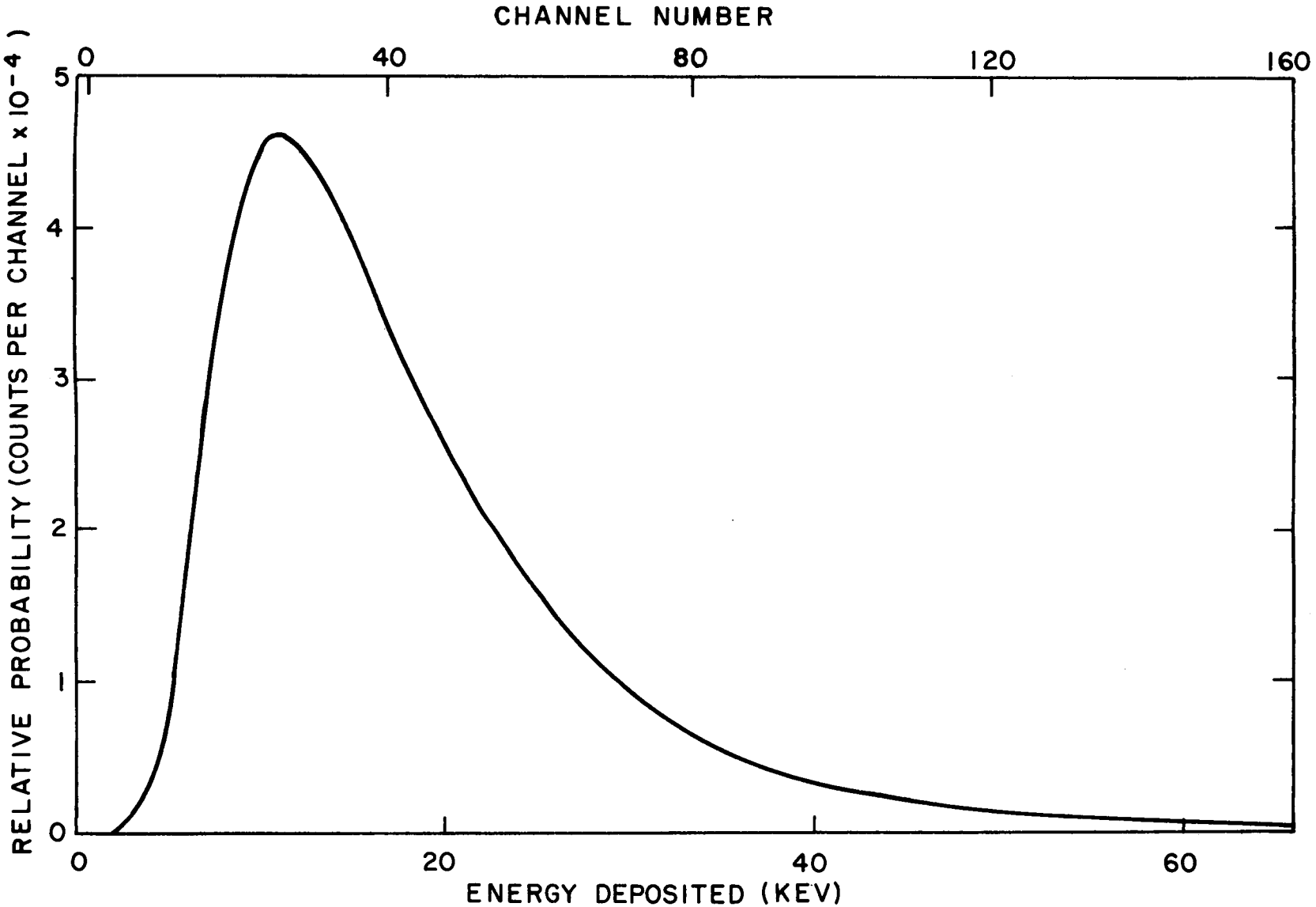

Figure 6. Energy deposition distribution in simulated 1.18 micron tissue-path, due to an incident proton energy spectrum with a peak at 43.0 MeV which has penetrated to a depth of 1.66 g/cm^2 in tissue-equivalent plastic (collimated proton beam).

range[2] of 1.67 g/cm^2 of tissue-equivalent plastic for 43 MeV protons, and with the 1.36% pathlength straggling (giving $\sigma \simeq 0.02$ g/cm^2) predicted by Janni.[3] It will be noted that the low energy side of the energy deposition

---

3. J. F. Janni, "Calculation of Energy Loss, Range, Path-length, Straggling, Multiple Scattering, and the Probability of Inelastic Nuclear Collisions for 0.1 to 1000 MeV Protons," AFWL-TR-65-150, Air Force Weapons Lab., New Mexico (1966).

---

peaks are essentially the same, as would be expected, since this part of the peak is due mainly to the numerous protons in the peak of the proton energy spectrum. There are, however, considerably more large depositions in the tails of the distributions produced by the collimated beam, contributed, of course, by the lower energy (and thus higher energy loss) protons in the spectrum.

Some of the experimental parameters are summarized in Table 1. The proton energies listed in the table are the calculated[2] residual energies of an incident 43.0 MeV proton after penetrating to the corresponding depths in tissue-equivalent plastic, and are included only to provide a feel for the magnitude of the proton energies corresponding to each energy deposition spectrum. It will be noted that the distributions retain their characteristic peaked shapes even at the largest depths examined, and that the widths of the distributions tend to decrease with depth and then increase again for even greater depths. Even though the last two peak widths in Table 1 are a measure of the wider collimated beam spectra, it is obvious from the data that this is a valid observation and has previously been observed in preliminary experiments. The widths of the

TABLE 1

Summary of Microscopic Energy Deposition Parameters for a 1.18 Micron Simulated Tissue Path (E_p = 43.0 MeV).

Depth in Tissue-Equivalent Plastic	Residual Energy of Incident 43 MeV Proton	Peak Width
g/cm^2	MeV	% FWHM
0.20	40.2	130
0.60	33.5	125
1.44	14.4	100
1.58[a]	8.2	117
1.66[a]	< 3[b]	133

[a] These Distributions were Obtained Using Collimated Beams.

[b] Range of 43 MeV Protons is $\simeq$ 1.67 g/cm^2 of Tissue-Equivalent Plastic.

distributions are, of course, determined by the combination of two effects; the fractional width tends to decrease as the mean energy of the incoming protons decreases (increasing the mean energy loss in the cavity), while the increasing energy spread of the proton spectrum tends to broaden the peak of the distribution. Such an interplay would be extremely difficult to predict theoretically.

It might be mentioned that the last two distributions are estimated to bracket the "Bragg-type" depth dose peak for 43 MeV protons. This estimate is based on two sources: (1) a properly scaled comparison with published depth dose data for 45 MeV protons,[4-6] and (2) the experimental observation

---

4. R. L. Tanner, N. A. Baily, and J. W. Hilbert, "Depth Dose Studies Using Monoenergetic Protons," Rad. Res. 27, #3, 540 (1966).
5. N. A. Baily, J. W. Hilbert, and R. L. Tanner, "High Energy Proton Dosimetry," 3rd International Congress of Rad. Res., Cortina D'ampezzo, 1966.
6. R. L. Tanner, N. A. Baily, and J. W. Hilbert, "High-Energy Proton Depth-Dose Patterns," Rad. Res. 32, 861-874 (1967).

---

by Raju[7] that, for a range of proton and alpha particle energies, the modal

---

7. M. R. Raju, "Heavy-Particle Studies with Silicon Detectors," UCRL-16613, Semi-Annual Report, Div. of Biology and Med., Lawrence Radiation Laboratory, Berkeley (1965).

---

energy at the Bragg-peak position is approximately 10 percent of the primary beam energy (however, cases in which this rather crude "rule-of-thumb" fails have recently been observed). It might also be mentioned that

a calculation of the theoretical energy-loss distribution for a 4 MeV proton shows that, because of the extremely thin tissue-path (1.18 microns) simulated here, the distribution is still quite far down into the Vavilov region ($K \simeq 0.14$).

The final set of measurements were made to illustrate the method by which the energy deposition distribution in a spherically (or arbitrarily) shaped microvolume may be determined and, in the process, to explore some of the implications of this method. The energy deposition distribution in a complete microvolume is approximated by measuring energy deposition distributions for a series of pathlengths and folding together these distributions on the basis of the relative number of pathlengths of each value seen by a parallel beam of protons incident on the particular volume. The volume most amenable to a simple interpretation is, of course, a sphere, which was originally analyzed by Rossi et al. In addition to having an isotropic directional response, a spherical volume results in a particularly simple distribution of pathlengths, given (for a parallel beam of incident radiation) by $P(x) = x/2r^2$, where r = sphere radius, and x = pathlength ($0 \leq x \leq 2r$). While there are obviously biological volumes of significance which may be more closely approximated by other shapes, only a spherically shaped volume will be treated in detail here, because of its relative simplicity, and implications to other shapes will be made in terms of the generalizations possible from the spherical example. The procedure for other volumes is, in principal, identical.

Energy deposition distributions were measured at pressures of 30.0, 25.0, 20.0, 15.0, 10.0, and 5.0 Torr, for protons having an energy of 40.0 MeV upon entering the sensitive gas volume of the tissue-equivalent proportional counter. These pressures simulate tissue paths of 1.77,

1.48, 1.18, 0.886, 0.590 and 0.295 microns, respectively, and the corresponding distributions were obtained using the coincidence requirements previously described. These energy deposition distributions are shown in Figures 7-12. It will be noted that a second set of axes have been provided for all of these curves, giving the absolute probability per keV of a given energy deposition versus the energy deposition in keV. This absolute normalization is obtained by graphically integrating the distributions (using a planimeter), and imposing the condition that the area under each curve is equal to 1.00 (i.e. the probability that a proton passing through the given pathlength loses some amount of energy, including zero, is unity). Ideally each experimental distribution should be integrated from zero to the energy of the incident proton (since there is an infinitesimally small probability of the proton losing its entire energy in the counter), or, more realistically, at least to the much smaller energy deposition corresponding to the maximum possible energy transfer to an atomic electron in a single collision ($\simeq$ 89 keV for 40.0 MeV protons). In practice, however, energy events of this magnitude are vanishingly infrequent, and the experimental distributions were integrated in each case to an energy deposition which is greater than 98% of the energy losses predicted by the Vavilov theory. Since some high energy delta rays may deposit only part of their energy in the counter, the energy-deposition distribution may have some events shifted from far out in the tail to smaller energies as compared to the corresponding energy-loss distribution. Therefore, the integration will include, if anything, an even greater percentage of all possible energy depositions, and thus represents a very good approximation to the total area. The properly normalized curves have been replotted in Figure 13 on a common scale to more clearly illustrate the manner in which the probability distributions

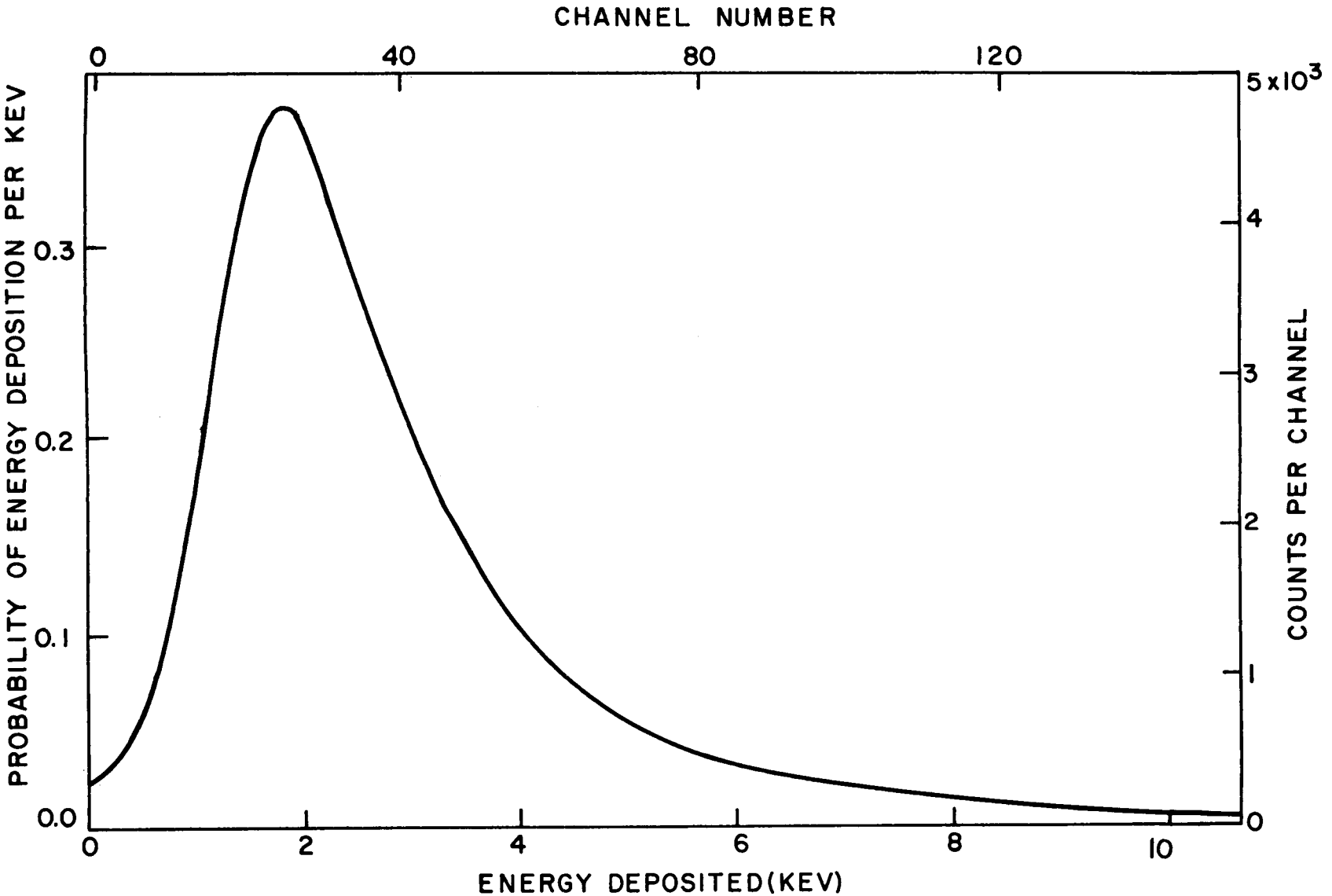

Figure 7. Normalized energy deposition distribution due to 40.0 MeV protons passing through a simulated tissue-path of 1.77 microns (30 Torr He-CO_2).

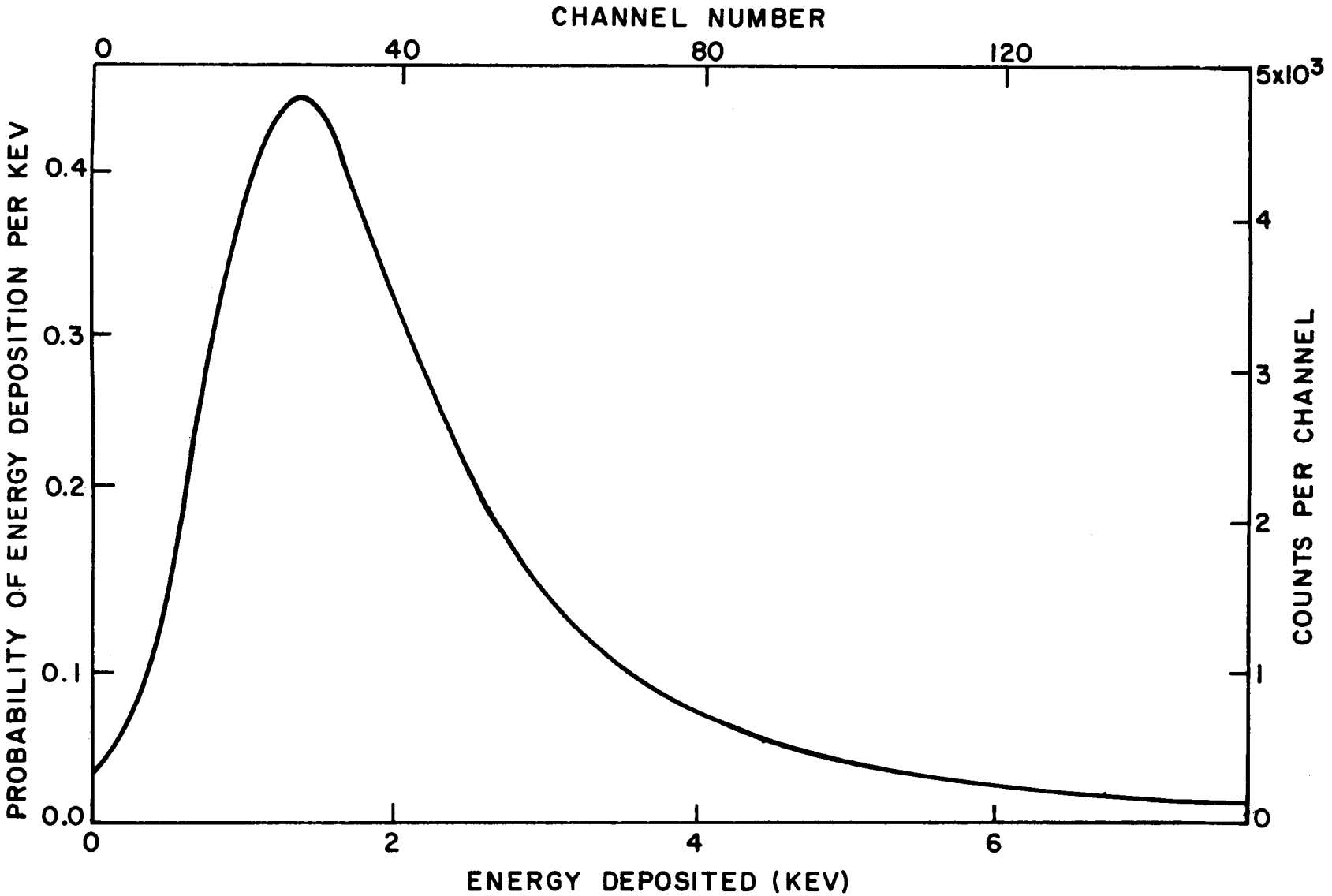

Figure 8. Normalized energy deposition distribution due to 40.0 MeV protons passing through a simulated tissue-path of 1.48 microns (25 Torr He-CO_2).

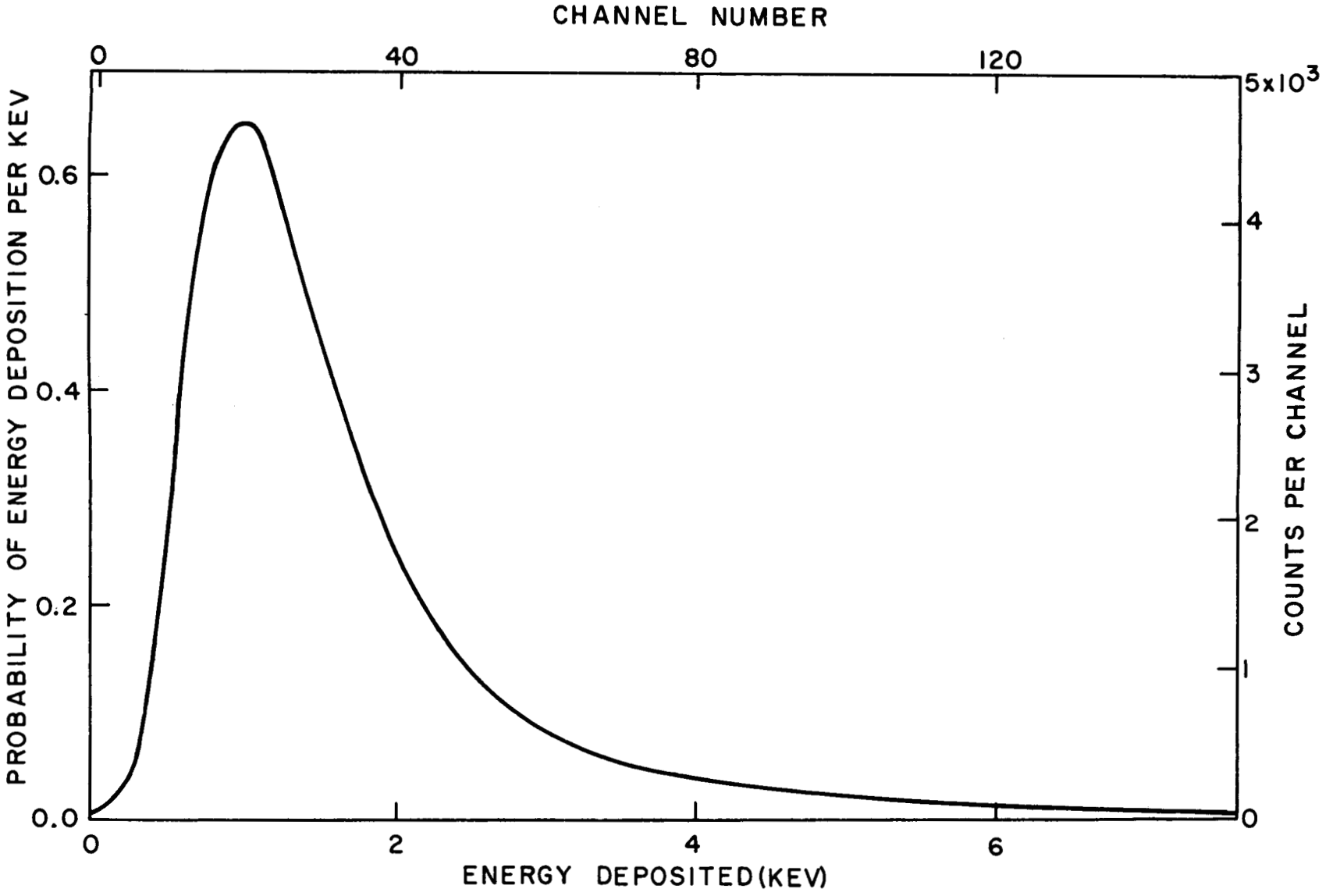

Figure 9. Normalized energy deposition distribution due to 40.0 MeV protons passing through a simulated tissue-path of 1.18 microns (20 Torr He-CO_2).

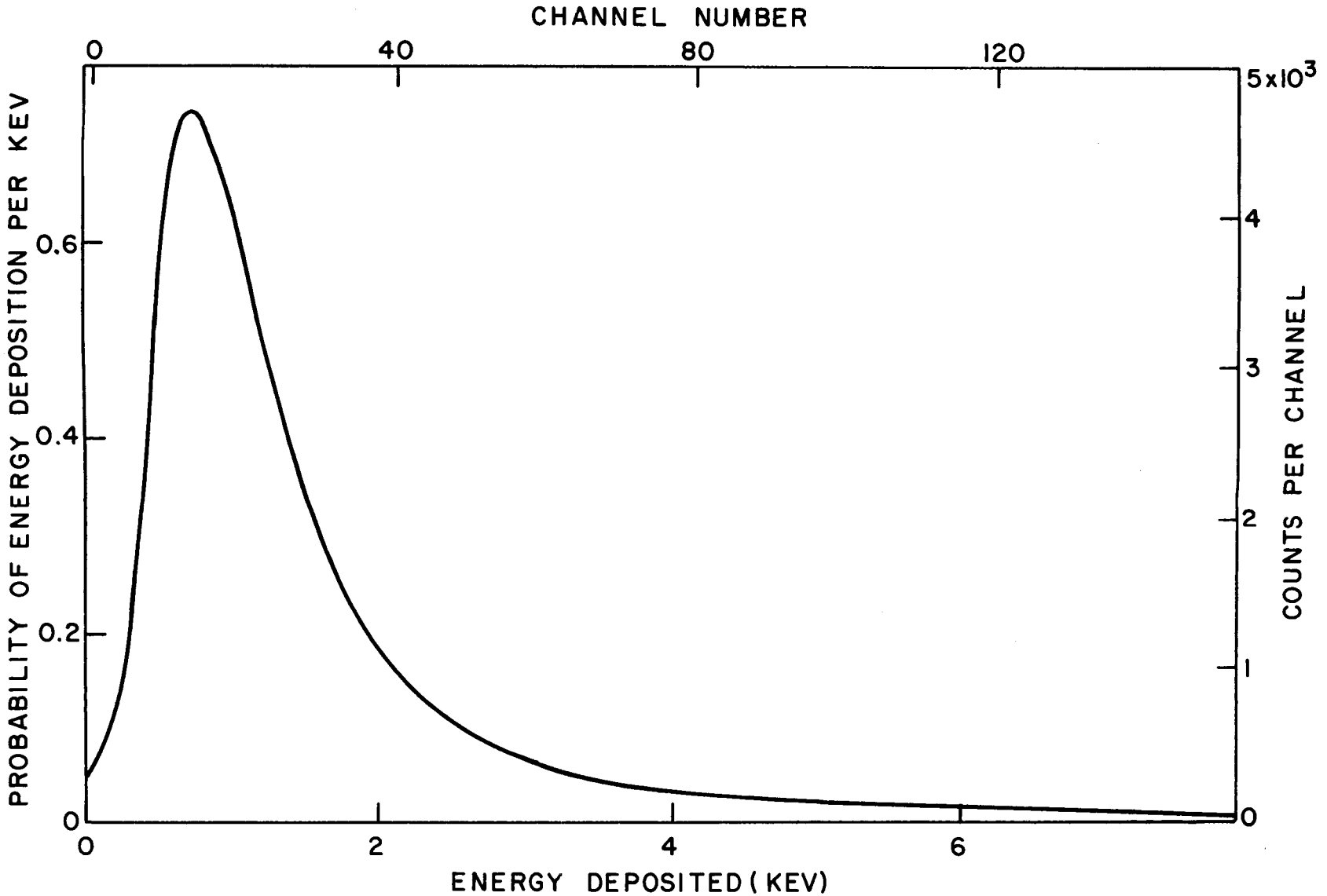

Figure 10. Normalized energy deposition distribution due to 40.0 MeV protons passing through a simulated tissue-path of 0.886 microns (15 Torr He-CO_2).

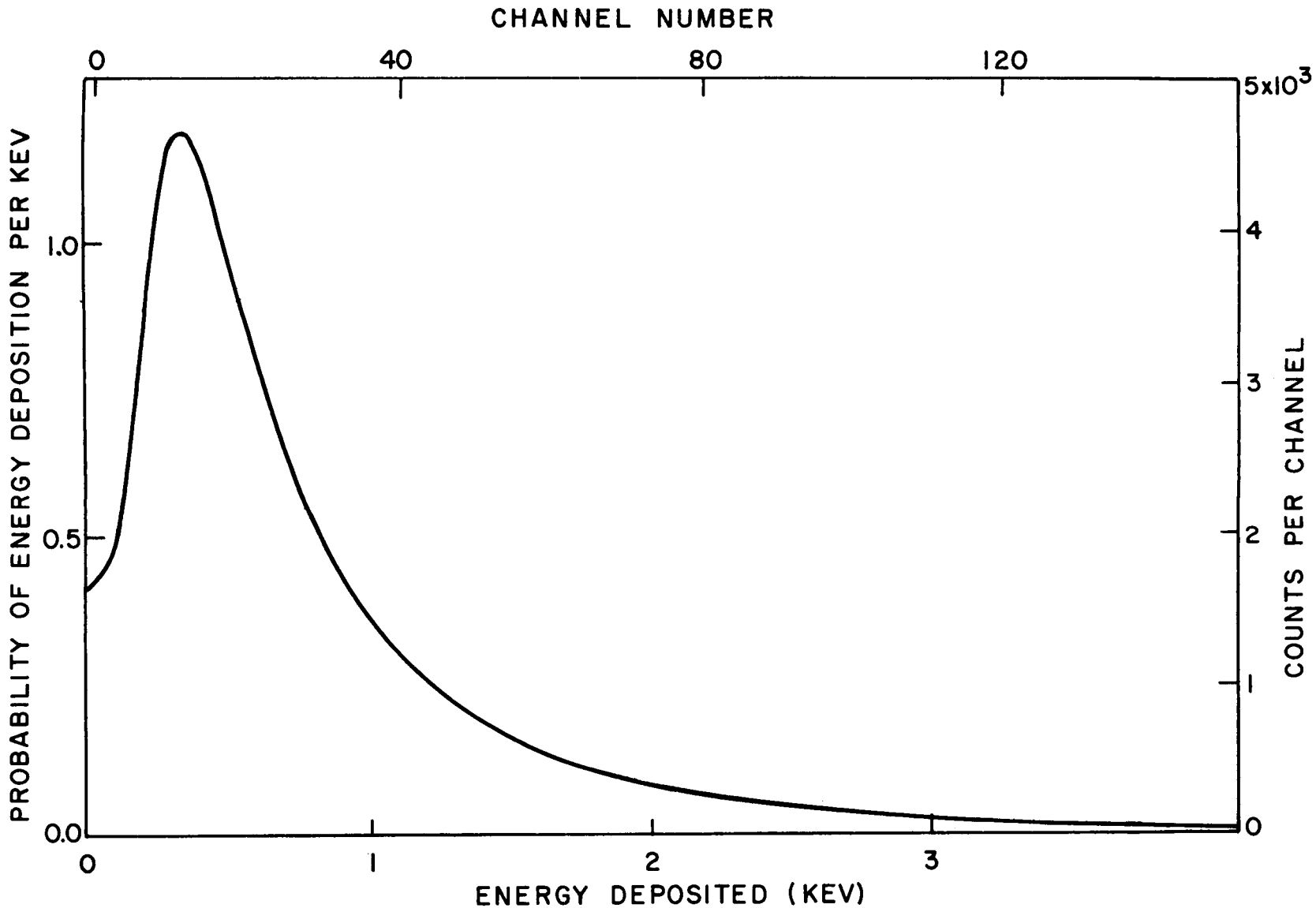

Figure 11. Normalized energy deposition distribution due to 40.0 MeV protons passing through a simulated tissue-path of 0.590 microns (10 Torr He-CO_2).

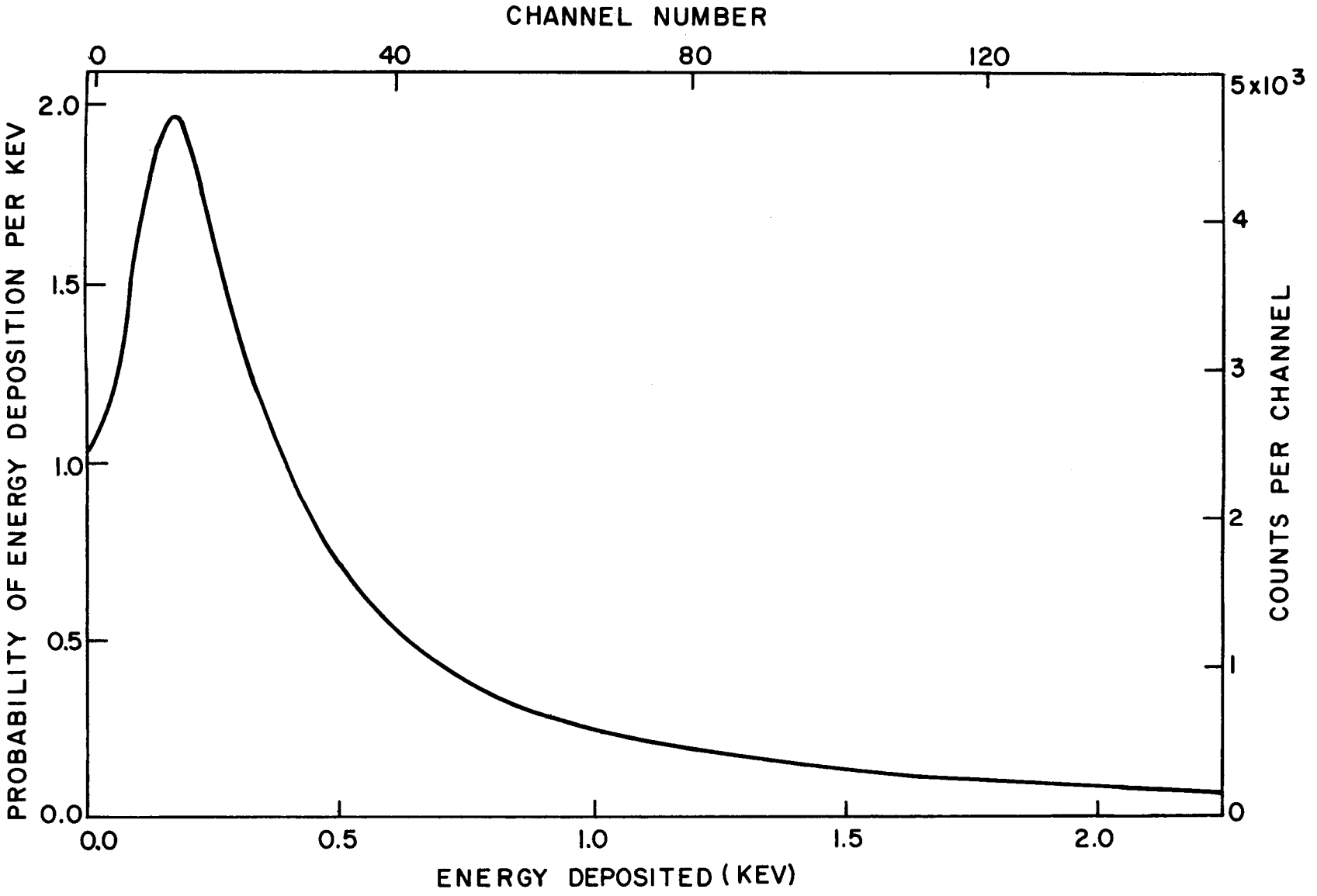

Figure 12. Normalized energy deposition distribution due to 40.0 MeV protons passing through a simulated tissue-path of 0.295 microns (5 Torr He-CO_2).

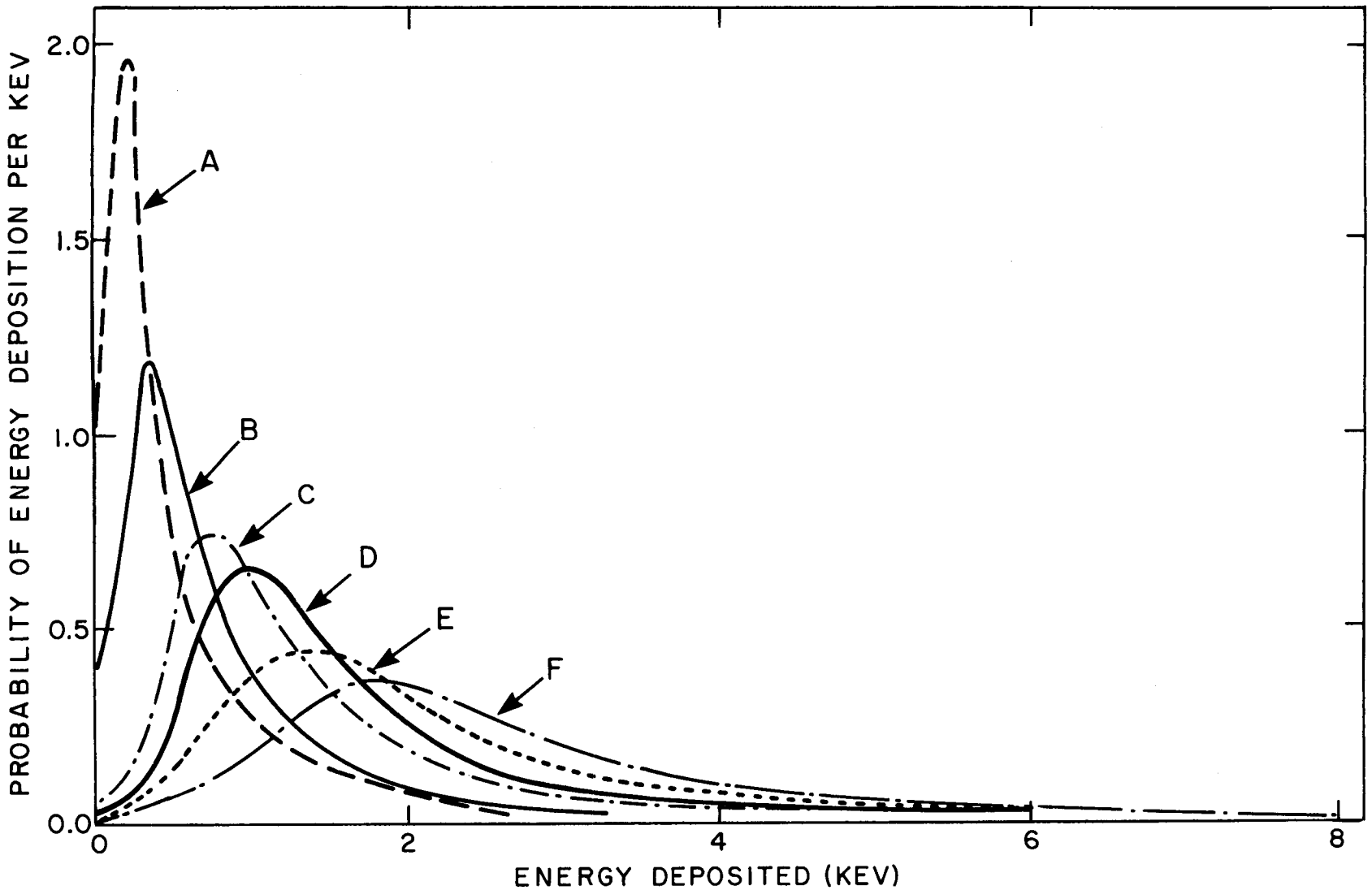

Figure 13. Probability distributions of energy deposition due to 40.0 MeV protons passing through various simulated tissue-paths. A = 0.295 microns; B = 0.590 microns; C = 0.886 microns; D = 1.18 microns; E = 1.48 microns; F = 1.77 microns.

change for the various simulated pathlengths. Probability values are next taken from the normalized curve for each pathlength, using a sufficiently fine energy grid, are weighted according to the relative number of each such pathlength in a spherical volume, and are added together to yield the probability distribution of energy deposition in the entire spherical microvolume, which has a diameter of 1.77 microns. This procedure, which is quite straightforward in concept, is rather tedious and timeconsuming when done by hand. For routine use of such a method, processing of the data by a computer program would obviously be highly desirable.

An obvious question relating to this method is how many individual pathlengths must be simulated to obtain a sufficiently accurate approximation to the distribution in an entire spherical microvolume. In order to examine this question, two composite distributions were constructed, one using all six simulated pathlengths, and a second using only three (0.59, 1.18, and 1.77 microns). The resulting distributions are shown in Figure 14. It might be mentioned that greater than 97% of all pathlengths existing in a 1.77 micron diameter sphere are included within the range of simulated pathlengths (0.295 to 1.77 microns). It will first be noted from Figure 14 that a marked discontinuity apparent at $\simeq$ 0.5 keV in the curve approximated by only three pathlengths, has essentially disappeared in the curve approximated by all six pathlengths. While no absolute quantitative conclusions can be drawn from the limited data available for this comparison, it is probably safe to say, judging from the relative change in the composite distribution upon increasing the number of simulated pathlengths from three to six, that for this particular distribution simulation of six pathlengths results in a reasonably good approximation to the distribution in the entire microsphere. This conclusion depends, of course, on the widths of the distributions

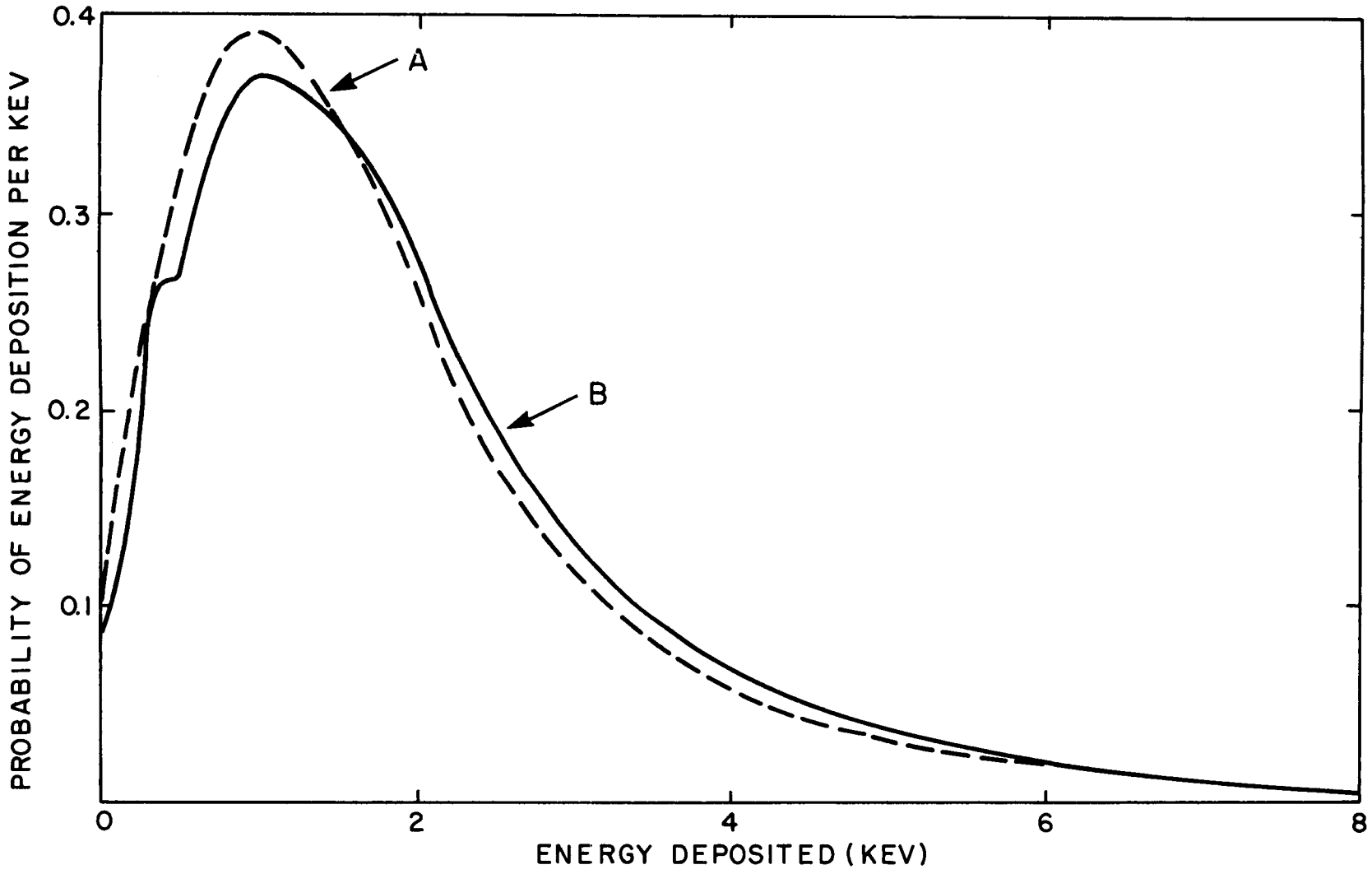

Figure 14. Probability distribution of energy deposition due to 40.0 MeV protons in a 1.77 micron diameter tissue microsphere. Curve A produced by summation of six pathlengths; curve B by summation of three pathlengths.

observed for each individual pathlength, the relatively small number of individual pathlengths required in this example being a result of the quite broad individual distributions. For much narrower individual distributions, such as would result if a much larger tissue microsphere were simulated, more individual distributions would be required, while for smaller simulated microspheres, which cases are much more likely to be of interest for distributions of this type, only a few would be necessary.

Kellerer in his approximate theoretical treatment of microdosimetric distributions, makes the generalization that, because of the very large statistical fluctuations in energy loss along individual pathlengths, the influence of the track length distribution in a volume is not decisive as long as the mean energy loss is less than several keV, so that similar results should be obtained with spherical and non-spherical volumes. Exactly what is implied quantitatively by this generalization is a question of interest. Since for the data presented here the mean energy loss in the maximum pathlength (i.e. the diameter) is approximately 2.6 keV, the data seems particularly well suited to examine this question. The simplest and most straightforward shape with which to make a comparison is simply a very thin slab, oriented perpendicular to the incident protons. Such a comparison is made in Figure 15, for a slab shaped volume which has a thickness equal to the average pathlength in the corresponding spherical volume. This average pathlength, for the triangular pathlength distribution which exists in a spherical volume, is just equal to 2/3 of the spherical diameter, or 1.18 microns. This is, very conveniently, just the pathlength simulated at 20 Torr, and this directly measured energy deposition distribution is the distribution (B) plotted in Figure 15. It will be noted that, while both distributions

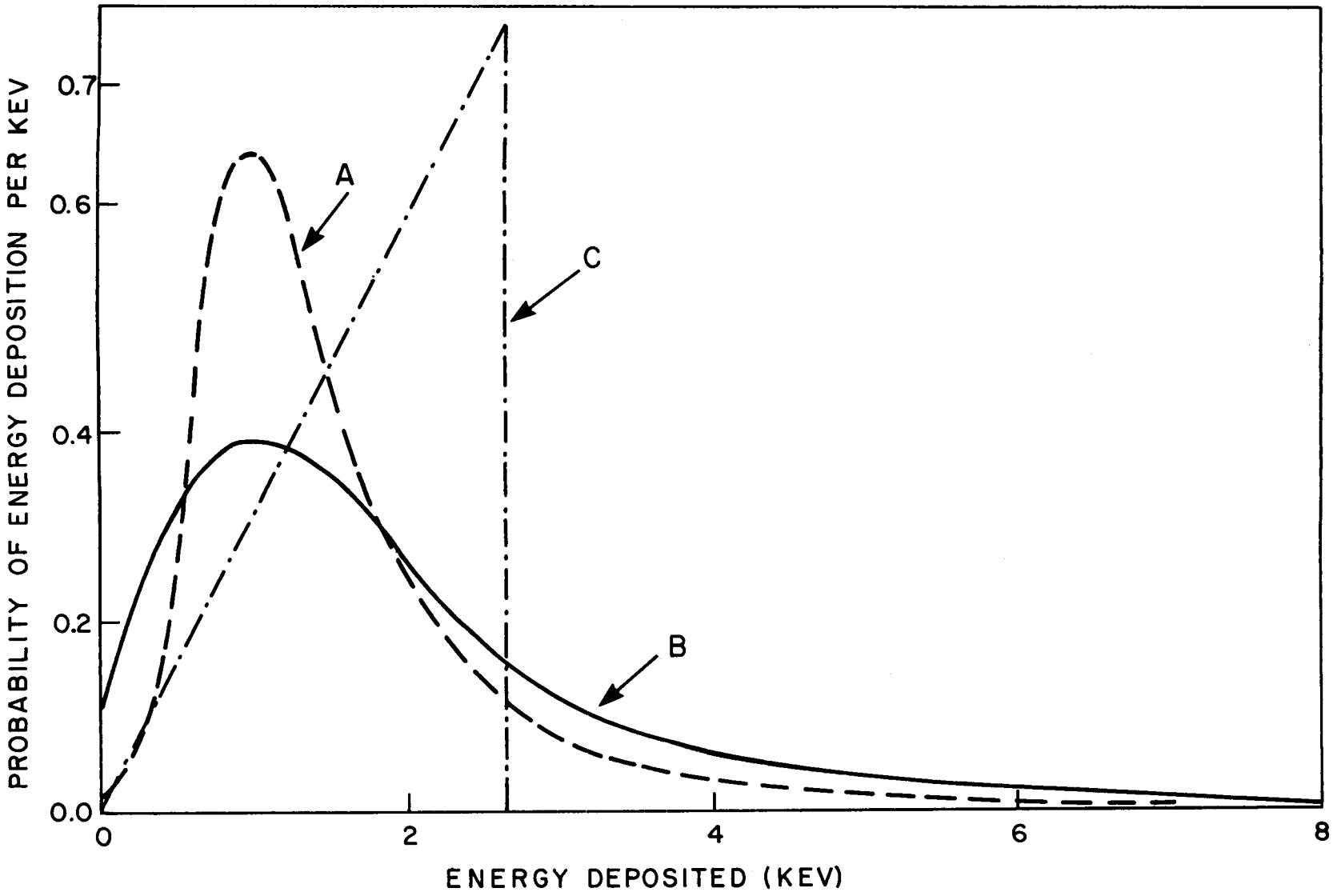

Figure 15. Various probability distributions of energy deposition, due to 40.0 MeV protons. A is in simulated 1.77 micron diameter tissue sphere; B is in 1.18 micron individual pathlength; C is theoretical distribution which would result if there were no statistical fluctuations of energy loss.

have the same characteristic "low-energy peak, high-energy tail" shape, and, in fact, peak at very close to the same energy deposition, quantitatively they differ greatly. Quantitative predictions relating to biological effects would be expected to differ greatly over a wide range for the two distributions, and thus it appears, from this example, that Kellerer's generalization is of little practical utility. The third curve displayed in Figure 15 illustrates, for comparison, the triangular energy-loss distribution which would be predicted for the 1.77 micron diameter microsphere if the statistical fluctuations in energy-loss of 43.0 MeV protons were completely ignored (i.e., if it were assumed that every proton passing through the microsphere experienced an energy-loss corresponding exactly to that predicted by the proton stopping power). The gross qualitative and quantitative difference of this distribution is obvious.

Energy Event Frequency Distributions

A more extensive analysis of the data appearing in the forthcoming Physical Review[8] article was undertaken so as to include the biologically important high energy tail. There are two important points to be investigated. First, is the agreement of this portion of the experimentally determined distribution with the Blunck-Leisegang corrected values of the Vavilov function. Second, from the point of view of radiobiological theories, the percentage of the macro dose delivered in single high

---

8. J. W. Hilbert, N. A. Baily, and R. G. Lane, "Statistical Fluctuations of the Energy Deposited in Low Atomic Number Materials by 43.7 MeV Protons," Phys. Rev. (in press).

---

energy events is important, since it will not only serve as a test for some existing theories but may aid in the formulation of modifications or even entirely new ones. Also, this is probably the most pertinent and direct way to predict a meaningful RBE. Only the first of these was investigated during the last six months.

In order to compare the experimental data with a completely corrected Vavilov distribution requires that a gaussian, whose width is determined by the Blunck-Leisegang parameter b and the quantity ξ, be folded into the Vavilov distribution.[9]

---

9. U. Fano, Ann. Rev. Nucl. Sci. 13, 1 (1963).

If the Vavilov function is denoted by $f_v(\Delta, x)$, then the corrected function is given by

$$f(\Delta, x) = (\xi b \sqrt{\pi})^{-1} \int_{-\infty}^{\infty} f_v(\Delta - U, x) \exp\left[-(U^2/\xi^2 b^2)\right] dU$$

Values of the Vavilov distribution function used were those of Seltzer and Berger,[10] with values of b taken from the graph given by Birkhoff.[11]

---

10. S. M. Seltzer and M. J. Berger, "Energy Loss Straggling of Protons and Mesons: Tabulation of the Vavilov Distribution," NAS-NRC, 1133, 205 (1964).

11. R. D. Birkhoff, "Distribution of Energy Losses-Straggling," Handbuch Der Physik, XXXIV, 87 (1958).

These distributions will then be normalized to those obtained experimentally so that they correspond at the value of the most probable

energy loss. In this manner a comparison of the high energy tail will be possible. Calculations have just been started so that no detailed comparisons have been made to date.

Papers Published

1. R. L. Tanner, N. A. Baily, and J. W. Hilbert, "High-Energy Proton Depth-Dose Patterns," Rad. Res. 32, 861-874 (1967).

2. N. A. Baily, W. M. Akutagawa, R. J. Andres, and H. L. Montano, "Some Characteristics of Lithium Drifted Silicon Structures," J. Appl. Phys. 38, 3907 (1967).

Papers Delivered

1. N. A. Baily and J. W. Hilbert, "Measurement of Frequency Distributions of Energy Absorbed in Small Volumes from High-Energy Protons," A.A.P.M. Annual Meeting, Dec., 1967.

Personnel

1. N. A. Baily, Ph.D. - Professor of Radiology
2. T. T. Robin, Ph.D. - Assistant Professor of Radiology
3. J. W. Hilbert, Ph.D. - Assistant Professor of Radiology

Plans for Next Period

During the next six months, we plan to pursue the following program:

1. Experimental data on energy event frequency distributions will be obtained, for protons having energies > 50 MeV, corresponding to those pathlengths of biological interest. From this data, distributions to be expected in spherical and cylindrical volumes will be computed.

2. A computer program to combine experimental energy event distribution curves in various geometries will be written and tested.

3. The comparison of the experimental data obtained at 43.7 MeV with theory over the whole range of energy events will be completed.

4. A redesigned proportional counter will be constructed. It is expected that the new design will facilitate its use at the cyclotron facilities.

5. A proportional counter gas which provides good tissue simulation at high proton energies will be tested in order to investigate contributions from such sources as would influence the energy event distributions in tissue.

6. The use of a bone-equivalent system will be investigated.

Appendix A

THE MEASUREMENT AND CHARACTERISTICS OF DEPTH DOSE PATTERNS DUE TO PROTON BEAMS*

Norman A. Baily
Department of Radiology, Emory University, Atlanta, Georgia

and

Harvey S. Frey
Department of Radiology, University of California at Los Angeles

ABSTRACT

The absorbed dose delivered to a particular organ or region of the body of an irradiated animal or human by a beam of high-energy protons depends upon such factors as: the organ or region under consideration, beam geometry, material through which the beam has passed prior to incidence on the subject considered, and other factors which may be peculiar to any pertinent situation. Of particular concern are regions in which rapid dose buildup may take place. A computer program was designed to utilize experimental depth dose data to produce isodose curves. These have been computed for proton energies between 45.8 MeV and 730 MeV in both circular and elliptical tissue equivalent cylinders irradiated over a 2 π geometry, by a parallel beam incident perpendicularly to the cylinder axis. The effect of passage through large thicknesses of copper and carbon before incidence on the cylinder has been investigated. The implication for physical dosimetry in light of the isodose patterns produced are discussed.

---

*Work supported in part by Grant #NGR-11-001-026, awarded by the Ames Research Laboratories, National Aeronautics and Space Administration.

INTRODUCTION

The problems associated with the proper and accurate measurement of depth dose received by persons or animals irradiated by beams of ionizing radiation have been of concern to physicists, physicians, and radiobiologists for many years. Many dosimetric studies involving x- and γ-rays, electrons and neutrons have been conducted during the past thirty years. These have included mapping isodose patterns in water, presdwood, and mix-D phantoms for beams having widely different energies, sizes, and angles of incidence. Corrections to isodose patterns for such perturbations as curvature of the incident surface, the use of wedge filters, rotation of the patient, passage of the beam through bone, air, and fat have all been studied. On the other hand, it has only been rather recently that heavy charged particle beams have been considered.

Various calculational techniques have been utilized in computer programs designed to assess the dose distributions produced by high energy protons. Wallace, et. al.,[1] computed the center line depth dose due to incident isotropic fluxes of monoenergetic protons (20 MeV to 730 MeV) in tissue-equivalent spheres. They included in their calculations the dose delivered both by primary and first-generation secondary protons.

An interesting analysis given in this paper[1] shows that the flux passing through the center of a sphere whose radius is d when an isotropic flux is incident over its surface is identical to that which would pass through a thin layer at a depth d in a flat slab when a

parallel beam is incident perpendicularly to its surface. Since the distance traveled in both cases is equal, the proton energy distributions will be identical, and therefore the dose delivered at the two points will be equal. If a straight ahead approximation is adapted, the same will be true for the dose delivered by the secondaries. However, this approximation requires further experimental study. Their calculations show that due to an increasing secondary (proton) contribution with proton (primary) energy and their range and depth of penetration, the center line depth dose patterns for high energy protons will depend upon both proton energy and sphere size. As an example, for 730 MeV protons, the portion of the total dose delivered by secondary protons is 14% for a 2.5 cm diameter sphere, 35% for a 10 cm diameter sphere, and 48% for a 25 cm diameter sphere. One can conclude that neither the production of secondary protons nor the geometry of the irradiated body can be neglected when the primary proton energy is greater than 100-200 MeV.

Comparisons of a revised calculational procedure[2] by the Berkeley group and experimental data[3] show good agreement at 730 MeV. In a later section, we shall discuss the results of a computer program designed to produce isodose curves from experimentally determined center line depth dose curves. The basic results obtained by Wallace, et. al.,[1] emphasize the influence of proton energy and the irradiation geometry on the dose patterns produced.

Steward[4] in a more recent report has included an exponential removal term for both primary and secondary protons to include the loss

of a portion of these particles with depth of penetration.

The distribution to be expected within an erradiated cylinder due to an incident parallel but broad beam was computed by Williams, et. al.,[5] for various proton energies. These calculations utilized the depth dose data calculated by Turner, et. al.[6]

There have been several experimental investigations of the dose patterns produced by high energy protons in low atomic number materials. Larsson[7] in discussing the use of 187 MeV protons for radiotherapeutic purposes points out the factors controlling the production and distribution of the Bragg peak. Perhaps even more significant was his observation that the depth dose distributions obtained with this beam depended upon beam width. Such a dependence has also been observed by one of us (NAB). However, quantitative data is not available. Other narrow beam data is available at 160 MeV.[8]

An illustration of some of the difficulties with which proton dosimetry is fraught is given by the work of Mitchell, et. al.,[9] and in the patterns to be discussed in a later section. It is, therefore, pertinent in view of the difficulties outlined above that the experimental determination of dose delivered by high energy charged particles, be they beams produced in the laboratory, or those due to the space environment, be carefully considered before choosing an experimental method for making such measurements.

The absorbed dose delivered to an irradiated object will depend upon many factors. Among the more important of these is the geometry of the irradiated body and the size of the incident beam. The

importance of these and other factors is a highly sensitive function of whether we are considering a parallel beam or isotropic radiation, and whether or not the beam has been perturbed by absorbers before incidence on the measuring system.

In order to correctly and accurately assess the dose distribution in man or animal, the measuring system (detector, or detector plus phantom) must simulate the irradiated system which one wishes to evaluate. This can always be done by an accurate geometrical representation of the irradiated body and placement of the measuring instrument at the appropriate position. However, in some cases a reasonably good approximation may be attained by a simpler configuration. The requirement is for the system to simulate both scattering and absorption characteristics. As will be seen, even curvature of the entrance surfaces will influence the depth dose patterns when absorption is important.

Of particular concern in experimental dosimetry programs are the regions in which rapid dose buildup takes place. For example, in the case of cascade protons, the number produced is proportional to the particle energy and the atomic weight of the medium through which it is passing. It is, therefore, possible in the case of bone to generate considerably more secondary protons thereby increasing the dose to deeper portions of the irradiated body. Similarly, the production of other secondaries, such as neutrons, depends on the primary proton energy and the interaction cross-section for the elements through which the beam passes.

Perhaps too often dismissed or overlooked is the possibility of Bragg peak dose buildup. While it is true that in simple geometries (spheres, cylinders) uniformly or isotropically irradiated that such buildups do not appear, the simple perturbation of changing from a circular cylinder to an elliptical cylinder makes it possible for protons having ranges less than the length of the major axis but greater than the minor axis to cause the appearance of "hot" spots or dose buildup regions where the absorbed dose is considerably greater than in the surrounding tissue. Similarly, surface dose buildup may also take place.

In either of these cases, the size and geometry of the detector is a critical parameter in acquiring an accurate assessment of dose in such regions.

RESULTS

A computer program was set up to use the data of Tanner, et. al.,[3] and from this data to compute the dose at the crossing points of a 1 cm grid across the cross-section of cylinders uniformly irradiated over a 2 π geometry, by a parallel beam incident perpendicularly to the axis of the cylinder. The results are expressed in terms of the surface dose which would be delivered by a broad beam whose central axis is perpendicular to a flat slab of tissue equivalent material. The computer program also computed the isodose curves. Some results for pure proton beams having energies of 45.8 MeV, 138 MeV, 300 MeV, 630 MeV, and 730 MeV are given in Tables 1-5. In the case of the elliptical cylinders, the columns labeled major, minor axis represent

the dose along these directions. Similarly, the column labeled 45^{o} represents the dose along a line midway between these axis.

Selected isodose curves computed for elliptical cylinders are shown in Fig. 1. Those for circular cylinders are concentric circles and except for the 45.8 MeV case can be generated from the tabular data. For this low energy the dose falls to zero at 2 cm depth in the case of a 10 cm diameter cylinder and to 35 rads/100 rads surface dose at this same depth in the 30 cm diameter cylinder.

The effect on depth dose patterns produced by the passage of high energy proton beams through large amounts of absorber is shown in Fig. 2. These curves are the center line depth dose curves produced by an essentially infinite area beam incident perpendicularly on a large flat slab. Curve A is for a beam having an initial energy of 730 MeV after passage through 199 g/cm^2 of carbon and having a final energy (computed)[10] of 220 MeV. Curve B is for the same beam after passage through 229 g/cm^2 of copper and having an energy of 260 MeV. These curves are distinctly different in two respects from those given by Tanner, et. al.[3] First, for the depths investigated ($\sim$ 30 cm), no peak in dose rate occurs. Second, the buildup of the higher energy beam is not as great as that for the lower. This is in contrast to the pattern found for pure proton beams. The behavior demonstrated can only be accounted for in terms of the secondary particle production being distinctly different in the two materials. Data similar to that given previously for pure and monochromatic proton beams are given for these beams in Tables 6 and 7. Isodose curves for elliptical

cylinders are shown in Fig. 3. Except for curve A, the isodose lines are at equal dose increments so that the area between the first isodose line shown and the surface has a dose intermediate between the surface value shown in the tables and that represented by this first line.

DISCUSSION

The computed isodose patterns are useful for two purposes. First, to aid the experimenter who is exposing or planning to expose large animals at cyclotron facilities, and second, to serve as a guide for persons planning dosimetry experiments at cyclotrons or in space vehicles.

One of the most striking patterns is that generated in the elliptical cylinder by the 138 MeV beam. The occurrence of the hot spot, which covers an area of some 6 x 8 cm, would include many vital organs. The dose here is 2.8 times that which would exist in the same region if the irradiated body had a circular cross-section and approximately 1.9 times that which would have been measured at a depth of 5 cm along the minor axis of the ellipse.

Surface dose rates delivered to the different cylinders by the same energy beam vary between 3% and 25%. At a depth of 1 cm, the dose rates vary between 1% and 22%, while at 5 cm, these vary between 1% and 24%. The largest deviations in all cases occur for the low energy beams. Since the majority of the proton flux expected to be encountered in manned space flight will have energies corresponding to those producing the largest errors, the use of heavy wall ionization

chambers in lieu of a phantom should be carefully considered. As already pointed out, the variation at the center of each of these configurations can be considerably larger when the Bragg peak ionization can be effective. Such effects may be possible at other depths for other beam energies. In all instances where sharp gradients may occur, it is mandatory to use small volume, low density devices.

The case of isotropic radiation such as might be expected in space is considerably more complicated. It seems likely that certain energies or spectra could produce isodose patterns which differ considerably for different measurement geometries.

CONCLUSIONS

1. Isodose curves produced by proton beams that cannot penetrate all dimensions of a phantom are dependent upon phantom geometry. This is true for measurements made at any depth in the phantom.

2. The use of heavy walled ionization chambers in lieu of realistic phantoms for depth dose measurements must be considered in terms of an acceptable measurement error.

3. The generation of extremely high dose rates is possible due to geometries in which the Bragg peak ionization is not smoothed over.

4. If at all possible measurements of dose due to high energy protons should be made in a realistic geometry and by sensors placed at anatomically important sites.

5. In many instances reliable measurements can only be obtained by the use of small volume detectors. These volumes must be small compared to the gradient in dose rate expected.

REFERENCES

1. R. Wallace, P. G. Steward, and C. Sondhaus, Primary and Secondary Proton Dose Rates in Spheres and Slabs of Tissue, UCRL-10980 Rev. (1964).
2. P. G. Steward, private communication.
3. R. L. Tanner, N. A. Baily, and J. W. Hilbert, Rad. Res. 32, 861 (1967).
4. P. G. Steward, Results of Computations of Depth Dose in Tissue Irradiated by Protons, UCRL-16154 (1965).
5. G. H. Williams, J. D. Hall, and I. L. Morgan, Rad. Res. 28, 372 (1966).
6. J. E. Turner, C. D. Zerby, R. L. Woodyard, H. A. Wright, W. E. Kinney, W. S. Snyder, and J. Neufeld, Health Phys. 10, 783 (1964).
7. B. Larsson, Brit. Jour. Rad. 34, 143 (1961).
8. T. V. Blosser, F. C. Maiensahein, and R. M. Freestone, Jr., Health Phys. 10, 743 (1964).
9. J. C. Mitchell, G. V. Dalrymple, G. H. Williams, J. D. Hall, and I. L. Morgan, Rad. Res. 28, 390 (1966).
10. S. M. Seltzer and M. J. Berger, Studies In Penetration of Charged Particles in Matter, NAS-NRC-1133, 187 (1964).

Table 1

Dose to selected points in cylinders irradiated by a 2 π symmetrical proton field uniform along its axis and having an energy of 45.8 MeV.

	Rads/100 Rads at Surface of a Flat Slab and Delivered by a Parallel Beam Incident Perpendicularly to the Surface				
Dose Point	10 cm dia. circular cylinder	30 cm dia. circular cylinder	Elliptical Cylinder: Major dia. = 30 cm Minor dia. = 20 cm		
			Major dia.	Minor dia.	45°
0	390	320	350	320	330
1 cm depth	400	350	390	360	330

Table 2

Dose to selected points in cylinders irradiated by a 2 π symmetrical proton field uniform along its axis and having an energy of 138 MeV.

	Rads/100 Rads at Surface of a Flat Slab and Delivered by a Parallel Beam Incident Perpendicularly to the Surface				
Dose Point	10 cm dia. circular cylinder	30 cm dia. circular cylinder	Elliptical Cylinder: Major axis = 30 cm Minor axis = 20 cm		
			Major dia.	Minor dia.	45°
Surface	710	570	630	590	630
1 cm depth	720	620	670	590	670
5 cm depth	730	680	730	670	870
Center	-	390	— 1,000 →		1,100* —

Table 3

Dose to selected points in cylinders irradiated by a 2 π symmetrical proton field along the cylinder axis. Proton energy equal 300 MeV.

	Rads/100 Rads at Surface of a Flat Slab and Delivered by a Parallel Beam Incident Perpendicularly to the Surface				
Dose Point	10 cm dia. circular cylinder	30 cm dia. circular cylinder	Elliptical Cylinder: Major axis = 30 cm Minor axis = 20 cm		
			Major axis	Minor axis	45°
Surface	690	700	690	700	710
1 cm depth	730	740	740	740	740
5 cm depth	750	760	760	760	760
Center	-	770	770		

Table 4

Dose to selected points in cylinders irradiated uniformly by a 2 π symmetrical proton field along the cylinder axis. Proton energy equal 630 MeV.

	Rads/100 Rads at Surface of a Flat Slab and Delivered by a Parallel Beam Incident Perpendicularly to the Surface				
Dose Point	10 cm dia. circular cylinder	30 cm dia. circular cylinder	Elliptical Cylinder: Major axis = 30 cm Minor axis = 20 cm		
			Major axis	Minor axis	45°
Surface	740	740	740	750	800
1 cm depth	820	830	830	840	830
5 cm depth	850	880	870	880	880
Center	-	890	890		

Table 5

Dose to selected points in cylinders irradiated uniformly by a 2 π symmetrical proton field uniform along the cylinder axis. Proton energy equal 730 MeV.

	Rads/100 Rads at Surface of a Flat Slab and Delivered by a Parallel Beam Incident Perpendicularly to the Surface				
Dose Point	10 cm dia. circular cylinder	30 cm dia. circular cylinder	Elliptical Cylinder: Major axis = 30 cm Minor axis = 20 cm		
			Major axis	Minor axis	45°
Surface	750	750	750	760	800
1 cm depth	860	850	850	870	860
5 cm depth	890	890	900	900	900
Center	-	910	910		

Table 6

Dose to selected points in long cylinders irradiated uniformly along and radially about the central axis. Data applies to a 730 MeV beam after passage through 199 g/cm^2 of carbon and having a mean energy of 220 MeV.

	Rads/100 Rads at Surface of a Flat Slab and Delivered by a Parallel Beam Incident Perpendicularly to the Surface				
Dose Point	10 cm dia. circular cylinder	30 cm dia. circular cylinder	Elliptical Cylinder: Major axis = 30 cm Minor axis = 20 cm		
			Major axis	Minor axis	45°
Surface	680	700	690	700	710
1 cm depth	710	730	720	730	730
5 cm depth	740	770	760	760	760
Center	-	780	770		

Table 7

Dose to selected points in long cylinders irradiated uniformly along and radially about the central axis. Data is for a 730 MeV beam after passage through 229 g/cm^2 of copper and having a mean energy of 260 MeV.

	Rads/100 Rads at Surface of a Flat Slab and Delivered by a Parallel Beam Incident Perpendicularly to the Surface				
Dose Point	10 cm dia. circular cylinder	30 cm dia. circular cylinder	Elliptical Cylinder: Major axis = 30 cm Minor axis = 20 cm		
			Major axis	Minor axis	45°
Surface	670	690	680	690	690
1 cm depth	690	710	700	710	710
5 cm depth	700	740	730	740	730
Center	-	750	740		

LIST OF FIGURES

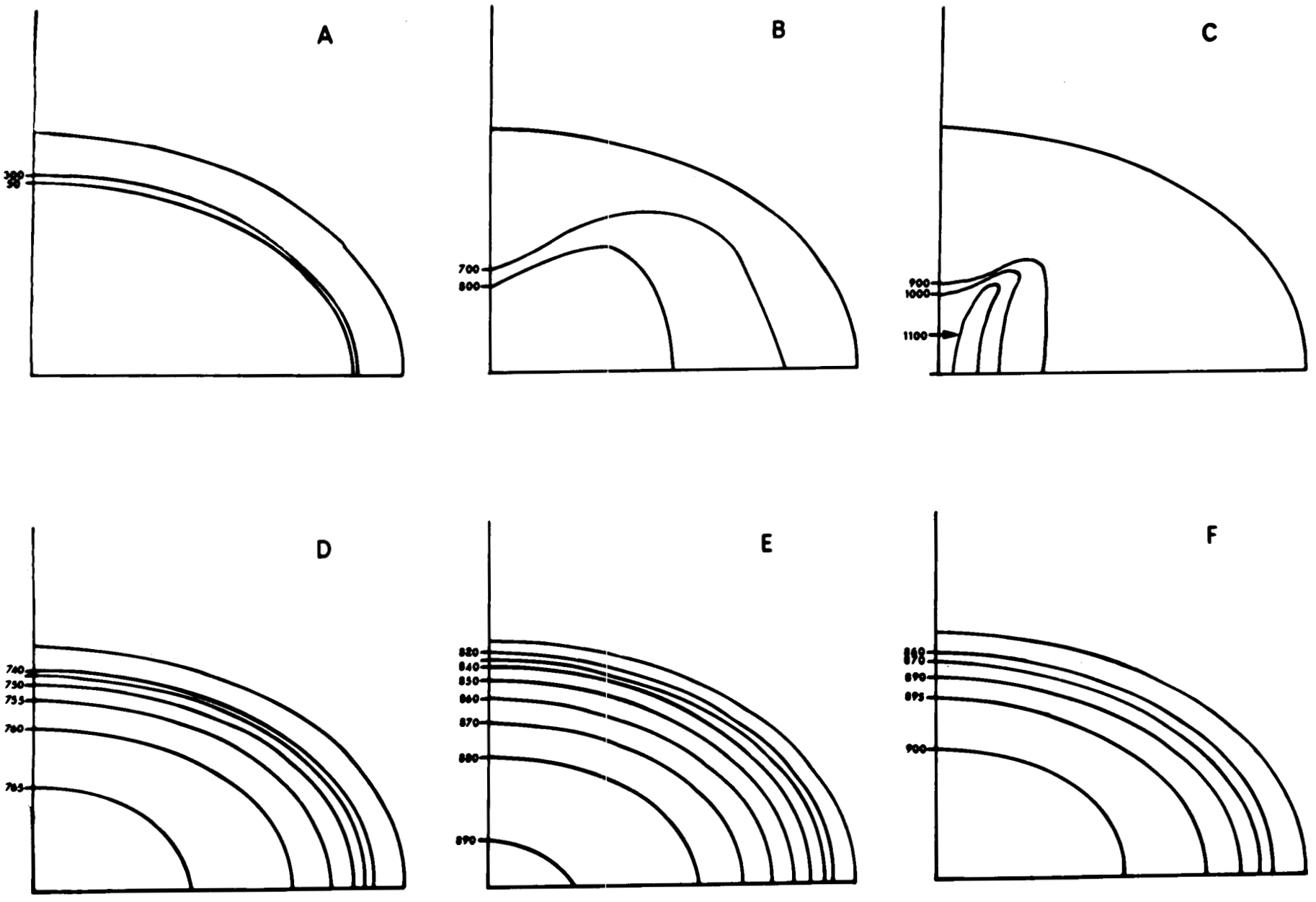

Figure 1.

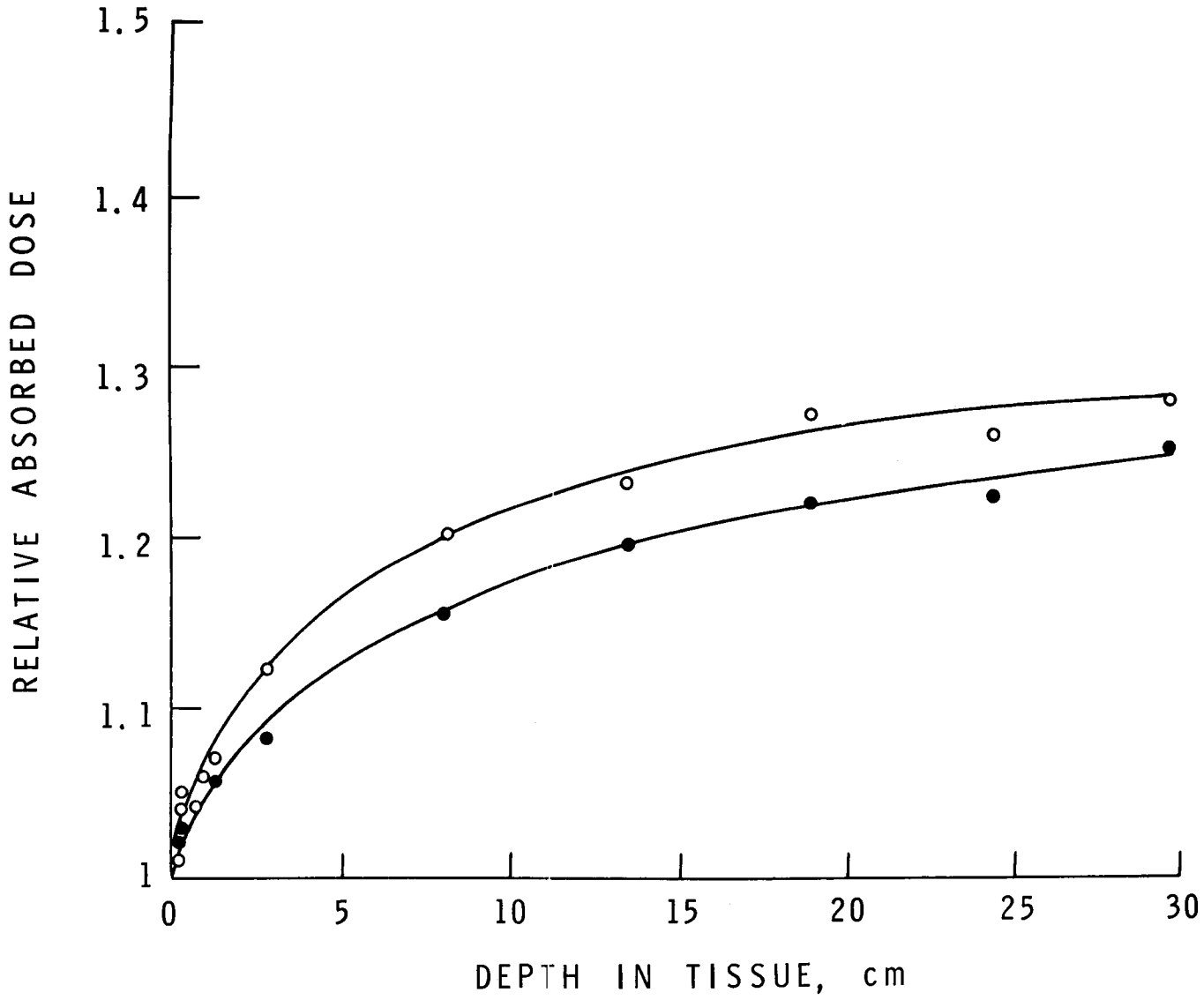
RELATIVE ABSORBED DOSE
1.5
1.4
1.3
1.2
1.1
1
0
5
10
15
20
25
30
DEPTH IN TISSUE, cm

Figure 2.

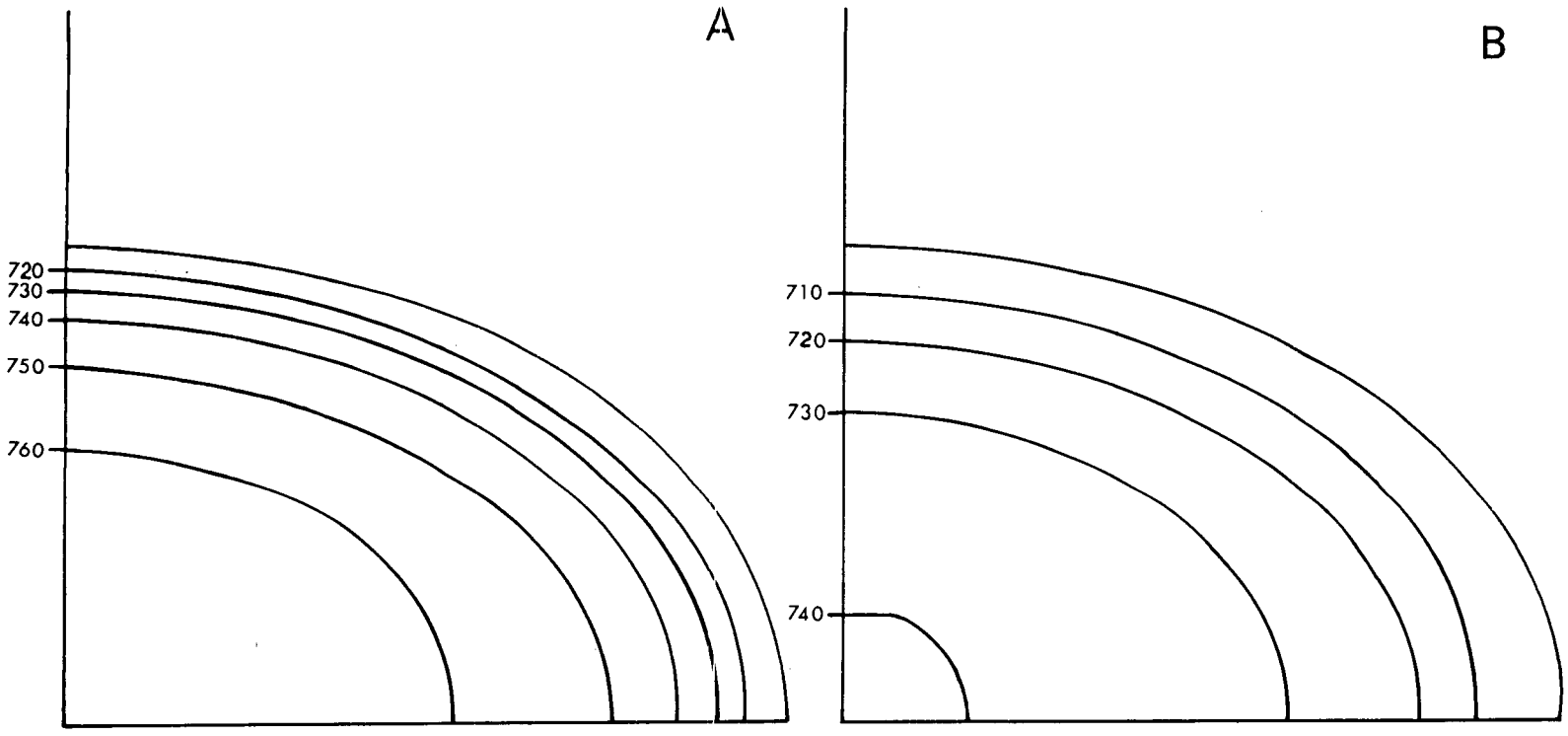

Figure 3.